

# MPCFormer: A physics-informed data-driven approach for explainable socially-aware autonomous driving

Jia Hu, Senior Member, IEEE, Zhexi Lian, Xuerun Yan, Ruiang Bi, Dou Shen, Yu Ruan, and Haoran Wang

**Abstract**— Autonomous Driving (AD) vehicles still struggle to exhibit human-like behavior in highly dynamic and interactive traffic scenarios. The key challenge lies in AD’s limited ability to interact with surrounding vehicles, largely due to a lack of understanding the underlying mechanisms of social interaction. To address this issue, we introduce *MPCFormer*, an explainable socially-aware autonomous driving approach with physics-informed and data-driven coupled social interaction dynamics. In this model, the dynamics are formulated into a discrete space-state representation, which embeds physics priors to enhance modeling explainability. The dynamics coefficients are learned from naturalistic driving data via a Transformer-based encoder-decoder architecture. To the best of our knowledge, MPCFormer is the first approach to explicitly model the dynamics of multi-vehicle social interactions. The learned social interaction dynamics enable the planner to generate manifold, human-like behaviors when interacting with surrounding traffic. By leveraging the MPC framework, the approach mitigates the potential safety risks typically associated with purely learning-based methods. Open-looped evaluation on NGSIM dataset demonstrates that MPCFormer achieves superior social interaction awareness, yielding the lowest trajectory prediction errors compared with other state-of-the-art approach. The prediction achieves an ADE as low as 0.86 m over a long prediction horizon of 5 seconds. Close-looped experiments in highly intense interaction scenarios, where consecutive lane changes are required to exit an off-ramp, further validate the effectiveness of MPCFormer. Results show that MPCFormer achieves the highest planning success rate of 94.67%, improves driving efficiency by 15.75%, and reduces the collision rate from 21.25% to 0.5%, outperforming a frontier Reinforcement Learning (RL) based planner.

This paper is partially supported by National Key R&D Program of China (2022YFE0117100), National Natural Science Foundation of China (Grant No. 52372317 and 52302412), Yangtze River Delta Science and Technology Innovation Joint Force (No. 2023CSJGG0800), Shanghai Automotive Industry Science and Technology Development Foundation (No. 2404), Xiaomi Young Talents Program, the Fundamental Research Funds for the Central Universities (22120230311), Tongji Zhongte Chair Professor Foundation (No. 000000375-2018082), and Shanghai Sailing Program (No. 23YF1449600). (Corresponding author: Haoran Wang)

Jia Hu, Zhexi Lian, Xuerun Yan, Ruiang Bi, and Haoran Wang are with Key Laboratory of Road and Traffic Engineering of the Ministry of Education, College of Transportation, Tongji University, No.4800 Cao’an Road, Shanghai, PR China, 201804. (e-mail: [hujia@tongji.edu.cn](mailto:hujia@tongji.edu.cn), [zhexi\\_lian@tongji.edu.cn](mailto:zhexi_lian@tongji.edu.cn), [frankyan@tongji.edu.cn](mailto:frankyan@tongji.edu.cn), [2431720@tongji.edu.cn](mailto:2431720@tongji.edu.cn), [wang\\_haoran@tongji.edu.cn](mailto:wang_haoran@tongji.edu.cn)).

Dou Shen and Yu Ruan are with Beijing Baidu Netcom Science Technology Co., Ltd, No. 8 Northeast Wangxi Road, Beijing, PR China, 100006. (e-mail: [shendou@baidu.com](mailto:shendou@baidu.com), [ruanyu@baidu.com](mailto:ruanyu@baidu.com)).

## I. INTRODUCTION

### A. Research motivation

During recent years, Autonomous Driving (AD) has demonstrated significant progress within transportation systems [1][2]. However, AD vehicles still face significant challenges in exhibiting human-like behavior in highly dynamic and interactive traffic scenarios such as off-ramp and unprotected left turns [3][4]. One critical reason is that AD vehicles lack the understanding of the underlying mechanisms of social interaction between surrounding vehicles. To be detailed, AD vehicles are not sure how surrounding vehicles will behave and how to react to the effects of surrounding vehicles’ behaviors. Given an illustrative example in Figure 1 (a), the ego AD vehicle attempts a lane change. But a lack of socially awareness makes it fail to understand and adapt motion cues of the surrounding vehicle [5], resulting in high safety risks. By contrast, in Figure 1 (b), a skilled human driver can recognize the potential behavior consequence of the surrounding vehicle and gives up the maneuver for safety. Hence, there is a great need to develop AD vehicles with socially-aware driving capability.

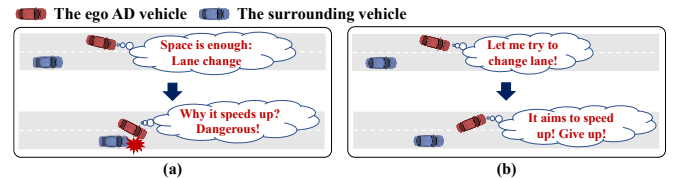


Figure 1 A lane-change maneuver comparison example between (a) the AD vehicle and (b) a skilled human driver.

### B. Related work and limitations

Current mainstream socially-aware autonomous driving approaches can be divided into three categories based on the development process: “passively”, “neutrally”, and “proactively” socially-aware approaches.

To enable the AD vehicle interacts effectively with other vehicles, early researchers developed Passively Socially-aware (PAS) approaches as shown in Figure 2 (a). This type of approach usually follows a hierarchical “prediction → reaction” fashion, which means predicting other vehicles’ trajectories firstly and passively reacting to the predicted trajectories secondly [6][7][8][9]. Consequently, to ensure safety in practice, the planned motions must avoid any conflicts with the predicted trajectories of other vehicles [10][11][12][13]. For instance, Wei et al [14] proposed a bi-level optimization framework grounded in game theory, wherein the AD vehicle’s motion planning is conditioned on the predictions of surrounding vehicles. In other words, the AD vehicles are constrained by predictions and have to yield

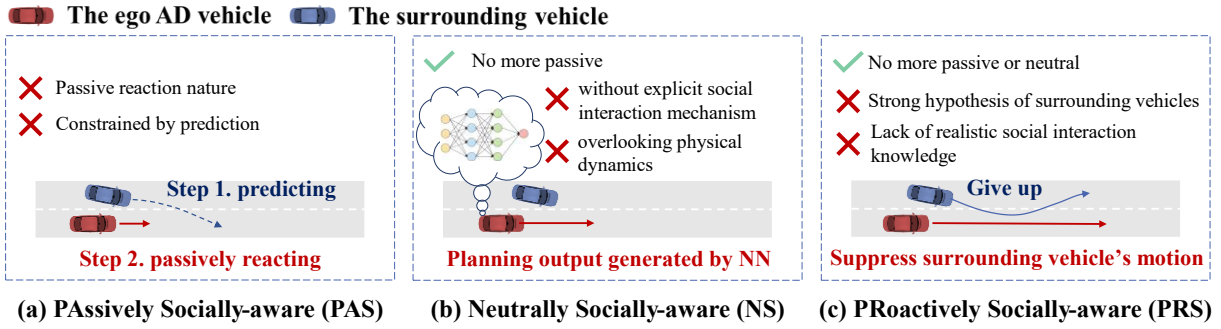


Figure 2 The illustration of current mainstream approaches and limitations.

TABLE I A detailed methodology comparison of existing socially-aware driving approaches.

Approach type	Research	Scenario	Based theory	Applied model
PAS	Eggert [6]	Collision avoidance	Rule-based	Time-to-X
	Werling et al [7]	Highway navigation	Sample-based	Quintic polynomials
	Sheng et al [8]	Crowd navigation	Search-based	POMDP
	Hubmann et al [9]	Merge	Search-based	POMDP+MCTS
	Li et al [10]	Parking	Optimization-based	MPC
	Zhou et al [11]	Highway navigation	Optimization-based	KF+MPC
	Huang et al [12]	City navigation	Learning-based	Transformer + QP
	Li et al [13]	Highway navigation	Learning-based	LSTM+QP
NS	Bronstein et al [18]	City navigation	Learning-based	Transformer+GMM
	Ye et al [19]	Highway navigation	Learning-based	DRL
	Hu et al [20]	Highway navigation	Learning-based	DRL
	Zhu et al [21]	Highway navigation	Learning-based	DRL
	Hu et al [23]	City navigation	Learning-based	MLP+GRU
PRS	Zhang et al [24]	Highway navigation	Game theory	IRL+MPC
	Hu et al [26]	Highway navigation	Game theory	IRL+MPC
	Goldendott and Leung [28]	Crowd navigation	Optimization-based	IBR+MPC
	Fan et al [27]	Intersection navigation	Learning-based	HRL
	Gharavi et al [25]	Collision avoidance	Optimization-based	SMPC

Notes: POMDP-- Partially Observed Markov Decision Process; MCTS-- Monte Carlo Tree Search; MPC-- Model Predictive Control; KF-- Kalman Filter; LSTM-- Long Short-Term Memory; QP-- Quadratic Programming; GMM-- Gaussian Mixture Model; DRL-- Deep Reinforcement Learning; MLP-- Mutiple Layer Perceptron; GRU-- Gated Recurrent Unit; IRL-- Inverse Reinforcement Learning; IBR-- Iterated Best Response; HRL-- Human-guided Reinforcement Learning; SMPC-- Stochastic Model Predictive Control.

to surrounding vehicles. Hence, the primary limitation of PAS approaches lies in its passive reaction nature, failing to proactively account for the behaviors of other vehicles. The generated motion planning trajectory must adhere to constraints imposed by the predicted trajectories of other vehicles. These constraints significantly narrow the solution space for motion planning, ultimately resulting in reduced planning effectiveness.

To overcome the passivity of PAS approaches, researchers have proposed Neutrally Socially-aware (NS) approaches as shown in Figure 2 (b). AD vehicles no longer react passively to surrounding vehicles in these approaches. Instead, they adopt an "environmental states input→Neural Networks (NN) → planning output" framework [15][16]. Through deep learning techniques, AD vehicles learn how to interact with surrounding vehicles and select motions based solely on the current and history environmental states. A key contribution is made by Chitta et al [17]. They used perception-fused attention blocks and autoregressive decoder for planned motion generation. However, two limitations still exist in NI approaches. Firstly, these approaches cannot explicitly explain social interaction mechanism between AD vehicles and surrounding vehicles. Because these approaches rely on black-box models [18][19], which just fit mapping laws from input

to output but fail to provide clear insights into how vehicles interact with each other [20]. Secondly, these approaches often overlook the underlying physical principles that govern vehicle dynamics. As these approaches often lack inherent consideration of vehicle dynamics [21][22][23], they potentially generate sudden and sharp maneuvers which exceed the vehicle's operational capabilities.

More recently, fewer researchers proposed PROactively Socially-aware (PRS) approaches as shown in Figure 2 (c). In order to achieve driving goals, these approaches can suppress the surrounding vehicles behaviors through proactive motions [24][25]. For instance, the ego AD vehicle could accelerate to narrow the following gap when surrounding vehicles attempt to cut in [26]. This proactive maneuver could discourage the potential cut-ins. While effective, one limitation in common has been raised. These approaches usually give strong behavior hypothesis of surrounding vehicles' behavior and lack inherent knowledge of social interaction mechanism. For instance, Zhang et al [24] developed a proactive motion planner with surrounding vehicles' behavior consideration and they assumed that surrounding vehicles are governed by a multi-objective cost function. However, when there is a significant behavior difference between the surrounding vehicles and the hypothesis, these approaches may fail to

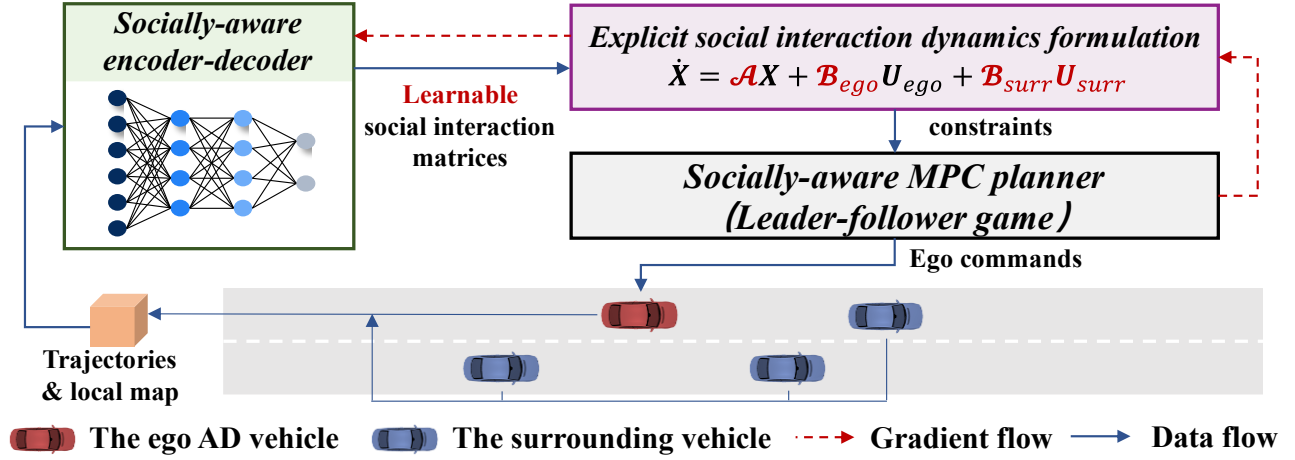


Figure 3 The overall architecture of the proposed approach

account for changes in the behavior of certain surrounding vehicles. This may lead to unforeseen conflicts or an inability to effectively avoid potential hazards [27][28].

### C. Contributions

To this end, we introduce *MPCFormer*, an explainable socially-aware autonomous driving approach with physics-informed and data-driven coupled social interaction dynamics. In this model, the dynamics are formulated into a discrete space-state representation, which embeds physics priors to enhance modeling explainability. The dynamics coefficients are learned from naturalistic driving data via a Transformer-based encoder-decoder architecture. To the best of our knowledge, MPCFormer is the first approach to explicitly model the dynamics of multi-vehicle social interactions. By integrating the learned social interaction dynamics into MPC planning based on a leader-follower game framework, the AD vehicle can generate manifold, human-like behaviors when interacting with surrounding traffic while mitigate the potential safety risks typically associated with purely learning-based approaches. The main contributions of the proposed approach are listed as follows.

*a) Our approach is the first to explicitly model the dynamics of multi-vehicle social interactions through a physics-informed data-driven modeling paradigm.* The proposed approach explicitly models the dynamics of social interactions among vehicles, termed as the explicit social interaction dynamics. To ensure explainability, we propose a physics-informed and data-driven coupled modeling paradigm. This paradigm formulates a state-space representation formula coupling behaviors of both the ego AD vehicle and the surrounding vehicles. Among the socially-aware system dynamics, each vehicle's state transition process is influenced not only by its own kinematic dynamics but also by social interaction effects from surrounding vehicles' behaviors. Hence, two types of components are integrated in the modeling paradigm: (1) physics-informed components which reflect vehicles' inherent physical kinematic dynamics; (2) data-driven components which reflect the social interaction effects between multiple vehicles. The data-driven components are explicitly modeled as learnable matrices, enabling them to capture and explain complex inter-vehicle social interaction

mechanism. To learn the data-driven components, we design a socially-aware Transformer-based encoder-decoder which fully exploits the social interaction mechanism embedded in natural driving data.

*b) Our approach enhances proactively socially-aware autonomous driving with explicit social interaction dynamics consideration.* The proposed approach integrates the explicit social interaction dynamics into the ego AD vehicle's MPC planning under a leader-follower game framework, enabling it to anticipate how various actions will trigger different reactions from surrounding vehicles. Hence, the ego AD vehicle can proactively plan its motions to achieve driving goals, while considering surrounding vehicles' all possible reactions.

*c) Our approach enables joint trajectory prediction and motion planning.* The proposed approach can integrate prediction into motion planning by setting the explicit social interaction dynamics as constraints in the MPC-based motion planning process. Hence, when optimizing motions of the ego AD vehicle within the future planning horizon, the future states of surrounding vehicles are also predicted simultaneously through the explicit social interaction dynamics. Hence, trajectory prediction and motion planning can be accomplished jointly.

## II. METHODOLOGY

### A. Overall architecture

The overall architecture of the proposed MPCFormer is shown in Figure 3. It consists of three modules:

- **Explicit social interaction dynamics formulation:** this module formulates the aforementioned explicit social interaction dynamics, in which both physics-informed vehicle kinematic and data-driven inter-vehicle social interactions are coupled modeled. The explicit social interaction dynamics serve as the constraints in the ego AD vehicle motion planning. The formulation process is detailed in Section II. B.

- **Socially-aware encoder-decoder:** this module utilizes trajectories and local maps of the ego AD vehicle and surrounding vehicles to generate the learnable dynamics coefficients (also called social interaction matrices) formulated in the aforementioned explicit social interaction dynamics. The inter-vehicle social interactions are fully

accounted in the proposed Transformer-based encoder-decoder structure. The structure of the encoder-decoder is detailed in Section II. C.

• **Socially-aware MPC planner:** this module designs an MPC-based motion planner for the ego AD vehicle. The planner can generate manifold, human-like behaviors through taking the explicit social interaction dynamics as the social interaction constraint based on a leader-follower game framework. It also mitigates the potential safety risks by hard collision avoidance constraints. The design of the planner is detailed in Section II. D.

### B. Explicit social interaction dynamics formulation

This section formulates the explicit social interaction dynamics. The social interaction effects between vehicles are considered as data-driven components in the dynamics and explicitly modeled as learnable matrices.

#### 1) Preliminary: single vehicle dynamics modeling

The single vehicle dynamics are served as the state transition model of the Ego AD Vehicle (EAV) and Surrounding Vehicles (SVs). Since EAV and SVs conducts longitudinal and lateral coupled maneuvers, the state vector is defined as:

$$\mathbf{x}_{ego} = (s_{ego}, v_{ego}, y_{ego}, \psi_{ego})^T \quad (1)$$

$$\mathbf{x}_{surr_i} = (s_{surr_i}, v_{surr_i}, y_{surr_i}, \psi_{surr_i})^T \quad (2)$$

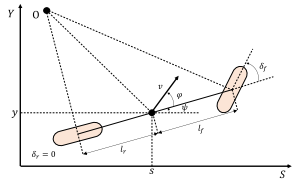
where  $\mathbf{x}_{ego}$  denotes the state of EAV and  $\mathbf{x}_{surr_i}$  denotes the state of SV  $i$ ;  $s_{ego}$  and  $s_{surr_i}$  are longitudinal positions of EAV and SV  $i$  under the Frenet coordinate;  $v_{ego}$  and  $v_{surr_i}$  represent the velocity of EAV and SV  $i$ ;  $y_{ego}$  and  $y_{surr_i}$  are lateral positions of EAV and SV  $i$  under the Frenet coordinate;  $\psi_{ego}$  and  $\psi_{surr_i}$  are the heading angles of EAV and SV  $i$ . The control inputs of EAV and SVs are defined as follows. It is worth noting that only EAV can be controlled proactively.

$$\mathbf{u}_{ego} = (a_{ego}, \delta_{f_{ego}})^T \quad (3)$$

$$\mathbf{u}_{surr_i} = (a_{surr_i}, \delta_{f_{surr_i}})^T \quad (4)$$

In Eq. (3) and (4),  $\mathbf{u}_{ego}$  denotes the control input of EAV and  $\mathbf{u}_{surr_i}$  denotes the control input of SV  $i$ ;  $a_{ego}$  and  $a_{surr_i}$  are the accelerations of EAV and SV  $i$ ;  $\delta_{f_{ego}}$  and  $\delta_{f_{surr_i}}$  are the front steering angles of EAV and SV  $i$ .

The vehicle system dynamics are modeled using the vehicle kinematic bicycle model [29]. As illustrated in Figure 4,  $\varphi$  is the angle of the current velocity of gravity center with respect to the longitudinal axis of the vehicle;  $l_r$  and  $l_f$  are distance between vehicle's gravity center and the rear and front axles respectively. The kinematic bicycle model is formulated as follows:



$$\begin{cases} \dot{s} = v \cos(\psi + \varphi) \\ \dot{y} = v \sin(\psi + \varphi) \\ \dot{\psi} = \frac{v}{l_r} \sin \varphi \\ \dot{v} = a \\ \varphi = \tan^{-1} \left( \frac{l_r}{l_r + l_f} \tan \delta_f \right) \end{cases} \quad (5)$$

Figure 4 Kinematic bicycle model notation.

Using the small angle assumption of  $\varphi$ , the kinematic bicycle model in Eq. (5) is linearized. Subsequently, the linear

vehicle system dynamics, which incorporates the kinematic models, can be derived as follows:

$$\dot{\mathbf{x}}_{ego} = \mathbf{A}_{ego} \mathbf{x}_{ego} + \mathbf{B}_{ego} \mathbf{u}_{ego} \quad (6)$$

$$\dot{\mathbf{x}}_{surr_i} = \mathbf{A}_{surr_i} \mathbf{x}_{surr_i} + \mathbf{B}_{surr_i} \mathbf{u}_{surr_i} \quad (7)$$

where,

$$\mathbf{A}_{ego} = \begin{bmatrix} 0 & 1 & 0 & 0 \\ 0 & 0 & 0 & 0 \\ 0 & 0 & 0 & v_{ego} \\ 0 & 0 & 0 & 0 \end{bmatrix}, \mathbf{A}_{surr_i} = \begin{bmatrix} 0 & 1 & 0 & 0 \\ 0 & 0 & 0 & 0 \\ 0 & 0 & 0 & v_{surr_i} \\ 0 & 0 & 0 & 0 \end{bmatrix} \quad (8)$$

$$\mathbf{B}_{ego} = \begin{bmatrix} 0 & 0 \\ 1 & 0 \\ 0 & 0 \\ 0 & \frac{v_{ego}}{l_r + l_f} \end{bmatrix}, \mathbf{B}_{surr_i} = \begin{bmatrix} 0 & 0 \\ 1 & 0 \\ 0 & 0 \\ 0 & \frac{v_{surr_i}}{l_r + l_f} \end{bmatrix} \quad (9)$$

#### 2) Explicit social interaction dynamics modeling

The explicit social interaction dynamics incorporate **social interaction effects** between EAV and SVs. For EAV and its SVs, the generalized state vector is defined as:

$$\mathbf{X} = (\mathbf{x}_{ego}, \mathbf{x}_{surr_1}, \dots, \mathbf{x}_{surr_n})^T \quad (10)$$

where  $\mathbf{X}$  is the system's state vector, which is a set of single vehicles' state vectors. The control input of the explicit social interaction dynamics can be also generalized from Eq. (2):

$$\mathbf{U}_{ego} = \left( \mathbf{u}_{ego}, \underbrace{\mathbf{0}, \dots, \mathbf{0}}_n \right)^T \quad (11)$$

$$\mathbf{U}_{surr} = (0, \mathbf{u}_{surr_1}, \dots, \mathbf{u}_{surr_n})^T \quad (12)$$

where  $\mathbf{U}_{ego}$  and  $\mathbf{U}_{surr}$  denotes control input of EAV and SVs respectively.  $\mathbf{U}_{surr}$  can be seen as reactions because it can be considered that SVs react to the EAV's motions.

Then, the explicit social interaction dynamics incorporate data-driven social interaction components between EAV and SVs. We introduce our discrete-time modeling paradigm as follows:

$$\mathbf{X}_{t+1} = (\mathbf{A}_t \Delta t + \mathbf{I}) \mathbf{X}_t + \mathbf{B}_{ego,t} \Delta t \mathbf{U}_{ego,t} + \mathbf{B}_{surr,t} \Delta t \mathbf{U}_{surr,t} + \mathbf{C}_t \Delta t (\mathbf{X}_t - \mathbf{X}_{t-1}) \quad (13)$$

where,

$$\mathbf{A}_t = \begin{bmatrix} \mathbf{A}_{ego,t} & \mathbf{0} & \dots & \mathbf{0} \\ \mathbf{0} & \mathbf{A}_{surr_1,t} & \dots & \mathbf{0} \\ \vdots & \vdots & \ddots & \vdots \\ \mathbf{0} & \mathbf{0} & \dots & \mathbf{A}_{surr_n,t} \end{bmatrix} \quad (14)$$

$$\mathbf{B}_{ego,t} = \begin{bmatrix} \mathbf{B}_{ego,t} & \mathbf{0} & \dots & \mathbf{0} \\ \mathbf{B}_{surr_1,ego,t} & \mathbf{0} & \dots & \mathbf{0} \\ \vdots & \vdots & \ddots & \vdots \\ \mathbf{B}_{surr_n,ego,t} & \mathbf{0} & \dots & \mathbf{0} \end{bmatrix} \quad (15)$$

$$\mathbf{B}_{surr,t} = \begin{bmatrix} \mathbf{0} & \mathbf{B}_{ego,surr_1,t} & \dots & \mathbf{B}_{ego,surr_n,t} \\ \mathbf{0} & \mathbf{B}_{surr_1,t} & \dots & \mathbf{B}_{surr_1,surr_n,t} \\ \vdots & \vdots & \ddots & \vdots \\ \mathbf{0} & \mathbf{B}_{surr_n,surr_1,t} & \dots & \mathbf{B}_{surr_n,t} \end{bmatrix} \quad (16)$$

$$\mathbf{C}_t = \begin{bmatrix} \mathbf{0} & \mathbf{C}_{ego,surr_1,t} & \dots & \mathbf{C}_{ego,surr_n,t} \\ \mathbf{C}_{surr_1,ego,t} & \mathbf{0} & \dots & \mathbf{C}_{surr_1,surr_n,t} \\ \vdots & \vdots & \ddots & \vdots \\ \mathbf{C}_{surr_n,ego,t} & \mathbf{C}_{surr_n,surr_1,t} & \dots & \mathbf{0} \end{bmatrix} \quad (17)$$

In Eq. (13),  $\Delta t$  denotes the discrete time interval;  $\mathbf{I}$  denotes diagonal unit matrix. The subscript  $t$  of each variable denotes the variable at time step  $t$ . It can be seen that the diagonal elements  $\mathbf{A}_{ego,t}, \mathbf{A}_{surr_1,t}, \dots, \mathbf{A}_{surr_n,t}$  of the state matrix  $\mathbf{A}_t$  are defined by the kinematic bicycle model, as illustrated in Eq. (8). These diagonal matrices reflect the vehicle's intrinsic kinematic properties. The same applies to diagonal matrices of  $\mathbf{B}_{ego,t}$  and  $\mathbf{B}_{surr,t}$  in Eq. (15) and Eq. (16). These matrices are the physics-informed vehicle kinematic component.

In Eq. (15-17), it can be seen that the off-diagonal matrices that explicitly reflect social interaction effects between vehicles. For instance,  $\mathbf{C}_{ego,surr_1,t}$  denotes the social interaction effect of SV  $i$  on EAV. The same applies to the control matrix  $\mathbf{B}_{ego,t}$  and  $\mathbf{B}_{surr,t}$  as well. These matrices are not derived from vehicle kinematics and can therefore be learned from natural driving data. Hence, the elements in  $\mathbf{A}_t, \mathbf{B}_{ego,t}, \mathbf{B}_{surr,t}$ , and  $\mathbf{C}_t$  can be classified into two categories which are physics-informed kinematic matrices and data-driven social interaction matrices, as shown in TABLE 2. The physics-informed kinematic matrices are pre-defined and the data-driven social interaction matrices need to be learned.

TABLE 2 State and control matrices classification.

Physics-informed kinematic matrices	$\mathbf{A}_{ego}, \mathbf{B}_{ego}$ $\mathbf{A}_{surr_1}, \mathbf{B}_{surr_1}$ ... $\mathbf{A}_{surr_n}, \mathbf{B}_{surr_n}$
Data-driven social interaction matrices	$\mathbf{C}_{ego,surr_1,t}, \dots, \mathbf{C}_{ego,surr_n,t}, \mathbf{B}_{ego,surr_1,t}, \dots, \mathbf{B}_{ego,surr_n,t}$ $\mathbf{C}_{surr_1,ego,t}, \dots, \mathbf{C}_{surr_1,surr_n,t}, \mathbf{B}_{surr_1,ego,t}, \dots, \mathbf{B}_{surr_1,surr_n,t}$ ... $\mathbf{C}_{surr_n,ego,t}, \dots, \mathbf{C}_{surr_n,surr_{n-1},t}, \mathbf{B}_{surr_n,ego,t}, \dots, \mathbf{B}_{surr_n,surr_n,t}$

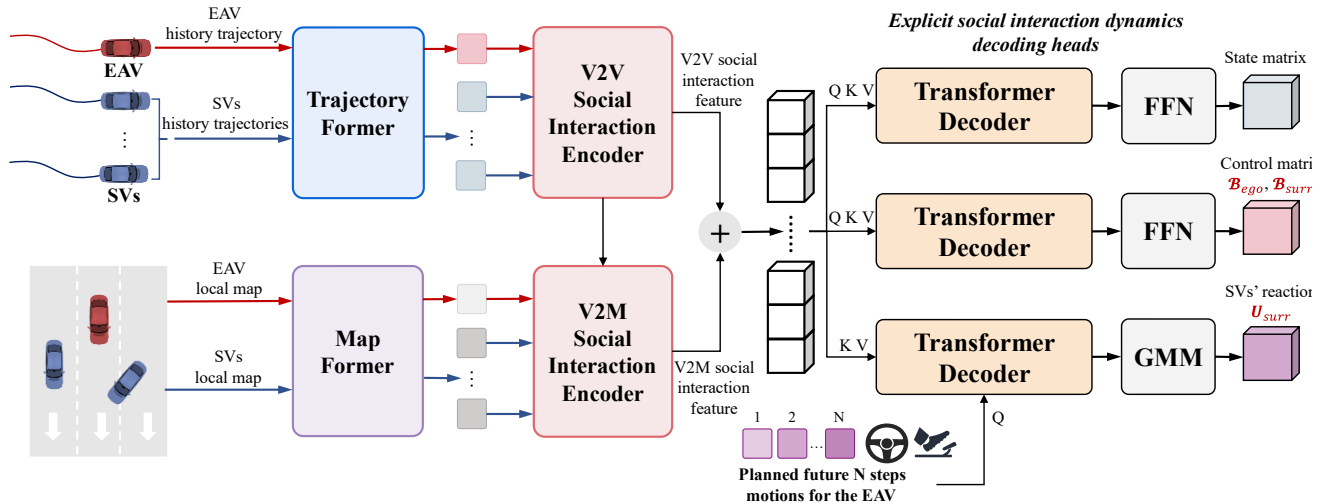


Figure 5 Illustration of the proposed socially-aware encoder-decoder

### C. Socially-aware encoder-decoder

In this section, this paper introduces how to learn the data-driven social interaction matrices in the explicit social interaction dynamics. We design a socially-aware Transformer-based encoder-decoder which fully exploits the social interaction mechanism between vehicles embedded in natural driving data. The whole structure of the socially-aware encoder-decoder is depicted in Figure 5.

#### 1) Input representation

The vehicle trajectory inputs contain the history trajectories of the EAV and SVs, defined as  $\mathbf{Traj}_{veh,t} \in \mathbb{R}^{T_h \times f_{veh}}$ ,  $veh \in \{ego, surr_1, \dots, surr_n\}$ , where  $T_h$  and  $f_{veh}$  denote the number of historical timesteps before current time step  $t$  and the number of trajectory features. The trajectory features include vehicle location, speed, acceleration, heading, and so on. The map inputs contain the map information in vehicle coordinates, termed  $\mathbf{Map}_{veh,t} \in \mathbb{R}^{3 \times L \times f_{map}}$ ,  $veh \in \{ego, surr_1, \dots, surr_n\}$ , where  $L$  and  $f_{map}$  denote the number of nearby waypoints and map features. The number 3 in the first dimension means three lanes are considered which are current lane, left lane, and right lane of the vehicle respectively.

#### 2) Social Interaction encoding

##### Vehicle-to-vehicle (V2V) social interaction encoding:

To encode the vehicle-to-vehicle social interaction, this paper firstly captures temporal attention of the single vehicle's trajectory through TrajectoryFormer in Figure 5. The TrajectoryFormer mainly relies on an ensemble of self-attention blocks:

$$\widehat{\mathbf{Traj}}_{veh,t} = \text{SelfAttn} \left( \begin{matrix} \text{MLP}(\mathbf{Traj}_{veh,t}), \text{MLP}(\mathbf{Traj}_{veh,t}), \\ \text{MLP}(\mathbf{Traj}_{veh,t}) \end{matrix} \right) \quad (18)$$

$veh \in \{ego, surr_1, \dots, surr_n\}$

$\widehat{\mathbf{Traj}}_{veh,t}$  is the processed temporal attention at time step  $t$ . SelfAttn is an ensemble of self-attention blocks and MLP is a sequence of multi-layer perceptrons. The query, key and value in the self-attention are all trajectory embeddings processed by MLP which aims to capture interaction effect among the trajectory set. Then this paper utilizes V2V Social Interaction Encoder to capture social interaction between

temporal attention of vehicles. This encoder is composed of an ensemble of cross-attention blocks:

$$\mathbf{V2V}_{veh_1 \rightarrow veh_2, t} = \text{CrossAttn} \left( \begin{array}{c} \widehat{\text{Traj}}_{veh_1, t}, \widehat{\text{Traj}}_{veh_2, t} \\ \widehat{\text{Traj}}_{veh_2, t} \end{array} \right)$$

$$veh_1, veh_2 \in \{ego, surr_1, \dots, surr_n\}, veh_1 \neq veh_2 \quad (19)$$

$\mathbf{V2V}_{veh_1 \rightarrow veh_2, t}$  denotes the social interaction feature reflecting interaction effect of  $veh_1$  on  $veh_2$  at time step  $t$ . CrossAttn is an ensemble of cross-attention blocks. It needs to be noted that this paper uses queries from  $veh_1$  to capture social interaction effect on  $veh_2$  through choosing keys and values from  $veh_2$ .

**Vehicle-to-map (V2M) social interaction encoding:** To encode the vehicle-to-map social interaction, this paper firstly processes the map information vector  $\mathbf{Map}_{veh}$  to embeddings using MLP, which forms MapFormer in Figure 5. Then this paper obtains the V2M social interaction feature through V2M Social Interaction Encoder. This encoder is also composed of an ensemble of cross-attention blocks:

$$\mathbf{V2M}_{veh_1 \rightarrow veh_2, t} = \text{CrossAttn} \left( \begin{array}{c} \mathbf{V2V}_{veh_1 \rightarrow veh_2, t}, \\ \text{MLP}(\mathbf{Map}_{veh_1, t}), \\ \text{MLP}(\mathbf{Map}_{veh_2, t}) \end{array} \right)$$

$$veh_1, veh_2 \in \{ego, surr_1, \dots, surr_n\}, veh_1 \neq veh_2 \quad (20)$$

$\mathbf{V2M}_{veh_1 \rightarrow veh_2, t}$  denotes the V2M social interaction feature reflecting interaction effect of  $veh_1$  on the local map of  $veh_2$  at time step  $t$ . To capture the V2M social interaction, this paper utilizes the  $\mathbf{V2V}$  social interaction feature  $\mathbf{V2V}_{veh_1 \rightarrow veh_2, t}$  as the queries and the map embeddings as the keys and values. That's because using the  $\mathbf{V2V}$  social interaction feature as the query can fully investigate the relationship between maps keys and values.

**Latent representation:** The latent representation  $\mathcal{Z}_t$  is obtained after the encoding process. It can be defined as:

$$\mathcal{Z}_t = \text{concat}(\{\mathbb{F}_{veh_1 \rightarrow veh_2, t}\})$$

$$veh_1, veh_2 \in \{ego, surr_1, \dots, surr_n\}, veh_1 \neq veh_2 \quad (21)$$

$$\mathbb{F}_{veh_1 \rightarrow veh_2, t} = \text{concat}(\mathbf{V2V}_{veh_1 \rightarrow veh_2, t}, \mathbf{V2M}_{veh_1 \rightarrow veh_2, t})$$

$$veh_1, veh_2 \in \{ego, surr_1, \dots, surr_n\}, veh_1 \neq veh_2 \quad (22)$$

where  $\mathbb{F}_{veh_1 \rightarrow veh_2, t}$  denotes the aggregated social interaction feature reflecting social interaction effect of  $veh_1$  on  $veh_2$ .

### 3) Explicit social interaction dynamics decoding

This paper designs three decoding heads as shown in Figure 5. The first and the second decoders are used to compute the data-driven social interaction matrices in state matrix  $\mathcal{C}$ , control matrix  $\mathcal{B}_{ego}$  and  $\mathcal{B}_{surr}$  respectively (modeled in Section II.B) in the future planning horizon  $N$ .

$$\mathcal{C}_{veh_1, veh_2, t}, \mathcal{C}_{veh_1, veh_2, t+1}, \dots, \mathcal{C}_{veh_1, veh_2, t+N-1} = \text{TransformerDecoderLayer}(\mathbb{F}_{veh_1 \rightarrow veh_2, t})$$

$$veh_1, veh_2 \in \{ego, surr_1, \dots, surr_n\}, veh_1 \neq veh_2 \quad (23)$$

$$\mathcal{B}_{veh_1, veh_2, t}, \mathcal{B}_{veh_1, veh_2, t+1}, \dots, \mathcal{B}_{veh_1, veh_2, t+N-1} = \text{TransformerDecoderLayer}(\mathbb{F}_{veh_1 \rightarrow veh_2, t})$$

$$veh_1, veh_2 \in \{ego, surr_1, \dots, surr_n\}, veh_1 \neq veh_2 \quad (24)$$

$$\begin{bmatrix} \mathcal{C}_t, \mathcal{C}_{t+1}, \dots, \mathcal{C}_{t+N-1} \\ \mathcal{B}_{ego, t}, \mathcal{B}_{ego, t+1}, \dots, \mathcal{B}_{ego, t+N-1} \\ \mathcal{B}_{surr, t}, \mathcal{B}_{surr, t+1}, \dots, \mathcal{B}_{surr, t+N-1} \\ \mathbf{U}_{surr, t}, \mathbf{U}_{surr, t+1}, \dots, \mathbf{U}_{surr, t+N-1} \end{bmatrix} = \text{SociallyAwareEncoderDecoder}_{\theta} \left( \begin{array}{c} \text{Traj}_{ego, t}, \dots, \text{Traj}_{surr_n, t} \\ \mathbf{Map}_{veh, t}, \dots, \mathbf{Map}_{surr_n, t} \\ \mathbf{U}_{ego, t}, \mathbf{U}_{ego, t+1}, \dots, \\ \mathbf{U}_{ego, t+N-1} \end{array} \right) \quad (25)$$

They are designed using typical Transformer Decoder Layers [30] as illustrated in Eq. (23) and (24).

The third decoder is used to compute the SVs' reactions  $\mathbf{U}_{surr}$ . Knowing that SVs react to the motions of EAV, this paper takes the planned future  $N$  steps motions of the EAV as the queries in the Transformer Decoder Layer to query the latent representation for SVs' reactions prediction. After that, this paper uses Gaussian Mixture Model (GMM) to compute  $M$  modalities of  $\mathbf{U}_{surr}$ , with average  $\hat{\mu}_{\mathbf{U}_{surr}}$ , variance  $\hat{\sigma}_{\mathbf{U}_{surr}}$  and probability  $\hat{p}$  of each modality. This paper selects the modality with the highest probability  $\hat{p}$ .

In summary, at each time step  $t$ , the operation of the socially-aware encoder-decoder can be abstracted as—— Given all vehicles' history trajectories, all vehicles' local maps, and EAV's planned motions to compute data-driven social interaction matrices of  $\mathcal{C}$ ,  $\mathcal{B}_{ego}$  and  $\mathcal{B}_{surr}$  and SVs' reactions  $\mathbf{U}_{surr}$  in the future horizon  $N$  as illustrated in Eq. (25), where  $N$  denotes the future horizon length;  $\theta$  denotes the parameters of the proposed socially-aware encoder-decoder.

### D. Socially-aware MPC planner

In this section, a socially-aware MPC planner is designed. It accounts for social interaction mechanism by considering the explicit social interaction dynamics as the constraint under a leader-follower game framework [31]. This design enables the planner to generate manifold, human-like behaviors when interacting with surrounding traffic while mitigate the potential safety risks.

**Definition 1:** For solving the socially-aware MPC planner in a rolling horizon fashion, some vector and matrix variables in future horizon dimension shall be defined as follows.  $N$  also denotes the discrete future horizon length.

$$\mathcal{X} = (\mathbf{X}_t, \mathbf{X}_{t+1}, \dots, \mathbf{X}_{t+N})^T \quad (26)$$

$$\mathbf{u}_{ego} = (\mathbf{U}_{ego, t}, \mathbf{U}_{ego, t+1}, \dots, \mathbf{U}_{ego, t+N-1})^T \quad (27)$$

$$\mathbf{u}_{surr} = (\mathbf{U}_{surr, t}, \mathbf{U}_{surr, t+1}, \dots, \mathbf{U}_{surr, t+N-1})^T \quad (28)$$

$$\bar{\mathcal{A}} = \begin{bmatrix} \mathbf{0} & \mathbf{0} & \dots & \mathbf{0} & \mathbf{0} \\ \mathcal{A}_t & \mathbf{0} & \dots & \mathbf{0} & \mathbf{0} \\ \mathbf{0} & \ddots & \ddots & \vdots & \vdots \\ \vdots & \mathbf{0} & \ddots & \mathbf{0} & \vdots \\ \mathbf{0} & \mathbf{0} & \dots & \mathcal{A}_{t+N-1} & \mathbf{0} \end{bmatrix} \quad (29)$$

$$\bar{\mathcal{B}}_{ego} = \begin{bmatrix} \mathbf{0} & \mathbf{0} & \dots & \mathbf{0} \\ \mathcal{B}_{ego, t} & \mathbf{0} & \dots & \mathbf{0} \\ \mathbf{0} & \ddots & \ddots & \vdots \\ \vdots & \mathbf{0} & \ddots & \mathbf{0} \\ \mathbf{0} & \mathbf{0} & \dots & \mathcal{B}_{ego, t+N-1} \end{bmatrix} \quad (30)$$

$$\bar{\mathbf{B}}_{surr} = \begin{bmatrix} \mathbf{0} & \mathbf{0} & \dots & \mathbf{0} \\ \mathbf{B}_{surr,t} & \mathbf{0} & \dots & \mathbf{0} \\ \mathbf{0} & \ddots & \ddots & \vdots \\ \vdots & \mathbf{0} & \ddots & \mathbf{0} \\ \mathbf{0} & \mathbf{0} & \dots & \mathbf{B}_{surr,t+N-1} \end{bmatrix} \quad (31)$$

$$\bar{\mathbf{c}} = \begin{bmatrix} \mathbf{0} & \mathbf{0} & \dots & \mathbf{0} & \mathbf{0} & \mathbf{0} \\ \mathbf{c}_t & \mathbf{0} & \dots & \mathbf{0} & \mathbf{0} & \mathbf{0} \\ -\mathbf{c}_t & \mathbf{c}_{t+1} & \ddots & \mathbf{0} & \vdots & \vdots \\ \vdots & \mathbf{0} & \ddots & \mathbf{c}_{t+N-2} & \mathbf{0} & \vdots \\ \mathbf{0} & \mathbf{0} & \dots & -\mathbf{c}_{t+N-2} & \mathbf{c}_{t+N-1} & \mathbf{0} \end{bmatrix} \quad (32)$$

$$\bar{\mathbf{D}} = (\mathbf{X}_t, \mathbf{0}, \dots, \mathbf{0})^T \quad (33)$$

$$\mathbf{Q} = \text{diag}(\theta_1, \theta_2, \theta_3, \theta_4, \underbrace{\mathbf{0}, \dots, \mathbf{0}}_{4n}) \quad (34)$$

$$\mathbf{R} = \text{diag}(\theta_5, \theta_6, \underbrace{\mathbf{0}, \dots, \mathbf{0}}_{2n}) \quad (35)$$

$$\mathbf{X}_{des} = (s_{des}, v_{des}, y_{des}, \psi_{des}, \underbrace{\mathbf{0}, \dots, \mathbf{0}}_{4n}) \quad (36)$$

where  $\mathbf{X}$ ,  $\mathbf{u}_{ego}$ , and  $\mathbf{u}_{surr}$  denote the state vector, control inputs of EAV, and control inputs of SVs in the future planning horizon respectively;  $\mathbf{u}_{surr}$  can be seen as the SV's reactions produced by the socially-aware encoder-decoder (Section II.C);  $\bar{\mathbf{A}}$ ,  $\bar{\mathbf{C}}$ ,  $\bar{\mathbf{B}}_{ego}$ , and  $\bar{\mathbf{B}}_{surr}$  are the state matrix and control matrices in the future planning horizon respectively.  $\mathbf{Q}$  and  $\mathbf{R}$  are coefficient matrices;  $\theta_1, \theta_2, \theta_3, \theta_4, \theta_5, \theta_6$  denote the weighting parameters used in the cost function;  $s_{des}, v_{des}, y_{des}, \psi_{des}$  denote the desired driving states of the EAV (position, speed, and heading angle).

### 1) Leader-follower game framework

This paper provides socially-aware and reliable motions based on a leader-follower game framework. Known as a kind of non-cooperative game, this framework is defined that the leader takes action first, and the follower reacts to the leader's action based on observations. For this paper, EAV could be accounted as a leader, while the SVs are treated as followers. The EAV anticipates the rational reactions of SVs and proactively optimizes its motions. SVs are assumed to react to EAV's motions. The socially-aware encoder-decoder anticipates their optimal reactions. The strategic social interactions between the EAV and SVs are embedded into a constrained optimization problem, expressed as shown in TABLE 3.

In TABLE 3,  $J_{EAV}(\mathbf{X}, \mathbf{u}_{ego})$  represents the EAV's driving cost;  $\mathcal{G}(\mathbf{X}, \mathbf{u}_{ego}, \bar{\mathbf{A}}, \bar{\mathbf{B}}_{ego}, \bar{\mathbf{B}}_{surr}, \bar{\mathbf{c}}, \mathbf{u}_{surr}) = \mathbf{0}$  denotes the explicit social interaction dynamics. By embedding SVs' reactions  $\mathbf{u}_{surr}$  and data-driven social interaction matrices  $\bar{\mathbf{C}}$ ,  $\bar{\mathbf{B}}_{ego}$ , and  $\bar{\mathbf{B}}_{surr}$  into the constraint set, this formulation maintains a tractable leader-follower game optimization structure in which **EAV optimizes its motions with consideration of SVs reactions and social interaction effects**. The implement details of the leader-follower game framework are illustrated in Figure 6. The socially-aware encoder-decoder provides anticipated SVs' reactions and other data-driven social interaction matrices (Section II.B) to formulate explicit social interaction dynamics constraint. The socially-aware MPC planner optimizes EAV's motions considering SVs' reactions. EAV, as the leader, takes action

TABLE 3 The constrained leader-follower game optimization problem.

#### The constrained leader-follower game optimization problem modeling

- 1: **Cost function:**  $\min J_{EAV}(\mathbf{X}, \mathbf{u}_{ego})$
- 2: **Constraints:**
- 3: Socially-aware constraint:  
 $\mathcal{G}(\mathbf{X}, \mathbf{u}_{ego}, \bar{\mathbf{A}}, \bar{\mathbf{B}}_{ego}, \bar{\mathbf{B}}_{surr}, \bar{\mathbf{c}}, \mathbf{u}_{surr}) = \mathbf{0}$
- 4:  $\bar{\mathbf{C}}, \bar{\mathbf{B}}_{ego}, \bar{\mathbf{B}}_{surr}, \mathbf{u}_{surr} = \text{SociallyAwareEncoderDecoder}_{\theta} \left( \begin{matrix} \text{Traj}_{ego,t}, \dots, \text{Traj}_{surr_n,t} \\ \text{Map}_{ego,t}, \dots, \text{Map}_{surr_n,t}, \mathbf{u}_{ego} \end{matrix} \right)$
- 5: Other constraints (collision avoidance, speed limit, ...)
- 6: **Solving:** any quadratic programming algorithm

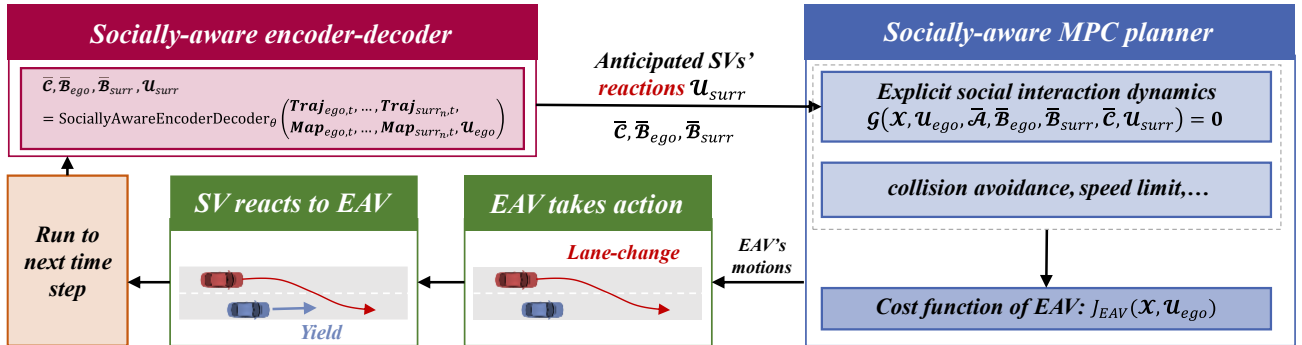


Figure 6 The leader-follower game framework

$$J_{EAV} = \frac{1}{2} \sum_{t=0}^{N-1} \left[ \underbrace{\theta_1 (s_{ego,t} - s_{des})^2}_{\text{longitudinal target}} + \underbrace{\theta_2 (v_{ego,t} - v_{des})^2}_{\text{driving efficiency}} + \underbrace{\theta_3 a_{ego,t}^2}_{\text{ride comfort}} + \underbrace{\theta_4 (y_{ego,t} - y_{des})^2}_{\text{lane-changing request}} + \underbrace{\theta_5 \psi_{ego,t}^2}_{\text{heading-changing smoothness}} + \underbrace{\theta_6 \delta_{f_{ego,t}}^2}_{\text{steering smoothness}} \right] \quad (37)$$

first. Then, SV, as the follower, conducts a reaction which completes the interactive cycle in the leader-follower game context. Finally, the whole process runs to the next time step.

## 2) Cost function

This paper designs a quadratic form of the cost function for the EAV as shown in Eq. (37). it reflects a combination of longitudinal and lateral driving goals. Taking a lane-changing maneuver as an example, first three terms drive the vehicle towards the target longitudinal position and speed while ensuring ride comfort. The fourth term drive the vehicle towards the target lane. The latter two terms confirm the heading-changing and steering smoothness. Then the cost function is converted to matrix form:

$$\min J_{EAV} = \frac{1}{2} [\mathbf{X}^T \quad \mathbf{u}_{ego}^T] \mathcal{P} \begin{bmatrix} \mathbf{X} \\ \mathbf{u}_{ego} \end{bmatrix} + \mathbf{q}^T \begin{bmatrix} \mathbf{X} \\ \mathbf{u}_{ego} \end{bmatrix} \quad (38)$$

where,

$$\mathcal{P} = \text{diag} \left( \underbrace{\mathbf{Q}, \dots, \mathbf{Q}}_N, \mathbf{0}_{5 \times 5}, \underbrace{\mathbf{R}, \dots, \mathbf{R}}_N \right) \quad (39)$$

$$\bar{\mathbf{C}}, \bar{\mathbf{B}}_{ego}, \bar{\mathbf{B}}_{surr}, \mathbf{u}_{surr} = \text{SociallyAwareEncoderDecoder}_{\theta} \left( \begin{matrix} \text{Traj}_{ego,t}, \dots, \text{Traj}_{surr_n,t} \\ \text{Map}_{ego,t}, \dots, \text{Map}_{surr_n,t}, \mathbf{u}_{ego} \end{matrix} \right) \quad (43)$$

TABLE 4 Collision avoidance constraints adding process

---

### Adding the collision avoidance constraints

---

- 1: **Initialize:** a large enough positive number  $M$ ; longitudinal safety distance reference  $s_{ref}$ ; lateral safety distance reference  $y_{ref}$ ; planning horizon  $N$
  - 2: **for**  $veh \leftarrow surr_1$  to  $surr_n$  **do:**
  - 3:   **for**  $j \leftarrow 1$  to  $N$  **do:**
  - 4:     Initialize a binary variable  $c_{veh,j} \in \{0,1\}$   
       Adding constraints to the planner:
  - 5:      $|s_{veh,j} - s_{ego,j}| \geq s_{ref} - M \cdot c_{veh,j}$   
        $|y_{veh,j} - y_{ego,j}| \geq y_{ref} - M \cdot (1 - c_{veh,j})$
  - 6:   **end for**
  - 7: **end for**
- 

### Algorithm 1 Learning & planning

---

**Require:** SociallyAwareEncoderDecoder $_{\theta}$ , planning steps  $N_p$ , training steps  $T_s$ , dataset  $\mathcal{DS}$

- 1: **for**  $j \leftarrow 1$  to  $N_t$  **do:**
  - 2:   Randomly sample a batch of data from dataset  $\mathcal{DS}$
  - 3:   Plan EAV's motions  $\mathbf{u}_{ego}$  to follow the ground-truth ego states
  - 4:   Predict  $\bar{\mathbf{C}}, \bar{\mathbf{B}}_{ego}, \bar{\mathbf{B}}_{surr}$  and  $\mathbf{u}_{surr}$  through SociallyAwareEncoderDecoder $_{\theta}$
  - 5:   Calculate system states  $\mathbf{X}$  using explicit social interaction dynamics
  - 6:   Calculate total loss  $\mathcal{L}$  according to Eq. (46)
  - 7:   Back-propagate loss and calculate gradients with respect to parameters  $\theta$
  - 8:   Update InteractionAwareEncoderDecoder $_{\theta}$
  - 9: **end for**
  - 10: Initialize the interactive simulation environment
  - 11: **for**  $t \leftarrow 1$  to  $N_p$  **do:**
  - 12:   Predict  $\bar{\mathbf{C}}, \bar{\mathbf{B}}_{ego}, \bar{\mathbf{B}}_{surr}$  and  $\mathbf{u}_{surr}$  using trained SociallyAwareEncoderDecoder $_{\theta}$
  - 13:   Plan EV's motion  $\mathbf{u}_{ego}$  using the proposed Socially-aware MPC planner
  - 14:   Execute the first step of the planned motion for EAV
  - 15: **end for**
- 

$$\mathbf{q} = \left( \underbrace{-\mathbf{Q}\mathbf{X}_{des}, \dots, -\mathbf{Q}\mathbf{X}_{des}}_N, 0, \dots, 0 \right)^T \quad (40)$$

## 3) Constraints

**Socially-aware constraint:** Under the leader-follower game framework, this paper accounts for social interaction mechanism by considering the explicit social interaction dynamics  $\mathcal{G}(\mathbf{X}, \mathbf{u}_{ego}, \bar{\mathbf{A}}, \bar{\mathbf{B}}_{ego}, \bar{\mathbf{B}}_{surr}, \bar{\mathbf{C}}, \mathbf{u}_{surr}) = \mathbf{0}$  as the constraint. This constraint incorporates the data-driven social interaction matrices and the reactions of SVs into the motion planning of EAV. This constraint is transformed to the dimension of the future optimization horizon:

$$\mathbf{X} = (\bar{\mathbf{A}} + \bar{\mathbf{C}})\mathbf{X} + \bar{\mathbf{B}}_{ego}\mathbf{u}_{ego} + \bar{\mathbf{B}}_{surr}\mathbf{u}_{surr} + \bar{\mathbf{D}} \quad (41)$$

then Eq. (41) is converted to align with the decision variables in Eq. (38).

$$\text{s. t. } [\bar{\mathbf{A}} + \bar{\mathbf{C}} - \mathbf{I} \quad \bar{\mathbf{B}}_{ego}] \begin{bmatrix} \mathbf{X} \\ \mathbf{u}_{ego} \end{bmatrix} + \bar{\mathbf{B}}_{surr}\mathbf{u}_{surr} + \bar{\mathbf{D}} = \mathbf{0} \quad (42)$$

The socially-aware encoder-decoder provides anticipated SVs' reactions and other data-driven social interaction matrices. It can be transformed from Eq. (25) as illustrated Eq. (43).

**Collision avoidance constraints:** This paper also accounts for collision avoidance using Big-M Method [32] as illustrated in TABLE 4. These constraints ensure that the EAV maintains either a longitudinal or lateral safe distance from SVs.

**Other constraints:** This paper also considers other constraints such as speed range, acceleration range, and heading range.

#### D. Learning & planning framework

This paper trains the socially-aware encoder-decoder proposed in MPCFormer using a natural driving dataset. During the forward pass, the proposed approach plans EAV motions to track the ground-truth ego states while predicting SVs' states via the explicit social interaction dynamics. In the backward pass, this approach evaluates the loss function on the predicted and planned states. The loss function includes vehicle state loss and GMM loss. Vehicle state loss is the smooth L1 error between the ground truth vehicle states and the predicted and planned states:

$$\mathcal{L}_{vehicles} = \text{SmoothL}_1(\mathbf{X} - \mathbf{X}_{groundtruth}) \quad (44)$$

The GMM loss is to minimize the variances of the selected  $\mathbf{U}_{surr}$  modality and the negative logarithm of the selected modality probability:

$$\mathcal{L}_{GMM} = \log(\hat{\sigma}_{\mathbf{u}_{surr}}) - \log(\hat{p}) \quad (45)$$

Hence, the loss function in the learning stage can be expressed as follows in which  $\lambda_1$  and  $\lambda_2$  are weighting factors:

$$\mathcal{L} = \lambda_1 \mathcal{L}_{vehicles} + \lambda_2 \mathcal{L}_{GMM} \quad (46)$$

In the planning stage, this paper conducts motion planning for accomplishing EAV's driving tasks in an interactive simulation environment. The motion planning is implemented in a rolling horizon fashion. Detailed learning & planning information is depicted in Algorithm 1.

### III. EVALUATION

The evaluation of the proposed MPCFormer is divided into two parts: i) open-looped prediction performance validation; ii) close-looped planning performance validation. The open-looped prediction is to validate the SVs' trajectory prediction performance of the proposed approach. The close-looped planning performance is to validate the EAV's planning performance.

#### A. Open-looped prediction performance validation

The open-looped prediction performance validation aims to answer the following questions: i) How is the proposed MPCFormer's prediction capability compared to existing

approaches? ii) Can the proposed MPCFormer actually enable explainable socially-aware predictions?

#### 1) Dataset preparation

In the learning stage, this paper adopts the Next Generation Simulation (NGSIM) dataset [33], covering a 640-meter section of US Highway 101 with five main lanes and an auxiliary lane between an on-ramp and an off-ramp as shown in Figure 8. This paper segments the whole dataset into frames. Each frame contains 9-s object tracks at 10 Hz which consist of 4-s history observation horizon and 5-s prediction horizon. Finally, this paper obtains 82608 frames for training & testing.



Figure 8 Data record area in US Highway 101.

#### 2) Measures of effectiveness

The following Measures of Effectiveness (MOE) are utilized for open-looped prediction performance validation:

- Average Displacement Error (ADE) and Final Displacement Error (FDE) is used to measure the predicting advantage of the proposed approach. ADE is defined as the average L2 norm distance between each point of the ground-truth trajectories and predicted trajectories. FDE is defined as the L2 norm distance between the final point of the ground-truth trajectories and predicted trajectories.

$$ADE = \frac{\sum_{n \in N} \sum_{t \in N_p} \|\hat{p}_t^n - p_t^n\|_2}{N \times N_p} \quad (47)$$

$$FDE = \frac{\sum_{n \in N} \|\hat{p}_{N_p}^n - p_{N_p}^n\|_2}{N} \quad (48)$$

where  $\hat{p}_t^n$  denotes the predicted position of vehicle  $n$  at time  $t$ ;  $p_t^n$  denotes the ground-truth position of vehicle  $n$  at time  $t$ .

- The predicted future trajectories SVs are used for prediction qualitative analysis and prediction explainability validation.

- The Frobenius norms of data-driven social interaction matrices are used for explicitly explain the social interaction strength between vehicles. It is defined as the square root of the sum of the absolute squares of all elements in a matrix. The higher value of the Frobenius norm indicates the higher social interaction strength between vehicles.

#### 3) Implementation details

This paper randomly selects 70% of processed data for training, 20% for validation, and 10% for testing. The training epoch is 25 and the learning rate is  $1 \times 10^{-3}$ . The model is trained on an NVIDIA RTX 4080 GPU with a batch size of 256. This paper trained the model for five times at different

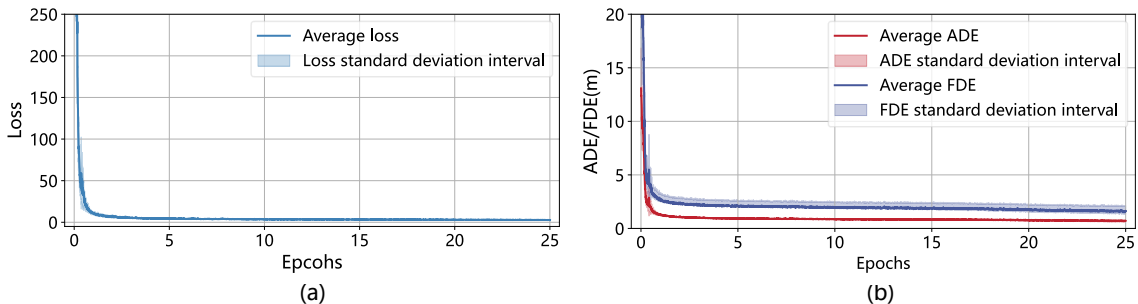


Figure 7 Learning process of the proposed socially-aware encoder-decoder. (a) Training loss; (b) The step-by-step ADE/FDE validation during training.

random seeds. The learning process is shown in Figure 7. Figure 7 (a) suggests that as the training proceeds, the average loss gradually decreases and converges. Figure 7 (b) suggests that the validated ADE and FDE also converge steadily. The results reflect the suitability of the model design for the problem.

#### 4) Baselines

The following baseline approaches are selected to compare with the proposed MPCFormer: **S-GAN** [34]: a multi-modal human trajectory prediction GAN trained with a variety loss to encourage diversity; **STGAT** [35]: a social spatial-temporal graph convolutional neural network for human trajectory prediction; **STM** [36]: a spatial-aware transformer for vehicle trajectory prediction; **HMNet** [37]: a hierarchical motion encoder-decoder network for trajectory forecasting; **PECNet** [38]: a VAE based model with goal conditioning predictions; **C2F-TP** [39]: a coarse-to-fine denoising framework for uncertainty-aware vehicle trajectory prediction; **SSTT** [40]: an interaction-aware trajectory prediction method based on sparse spatial-temporal transformer.

#### 5) Quantification results

This subsection aims to answer the first question. The open-looped prediction performance is quantified through prediction errors as shown in TABLE 5. Results show that the proposed MPCFormer exhibits strong robustness for both short-term and long-term predictions. It can be seen that the proposed MPCFormer outperforms most approaches across all time horizons, achieving the lowest prediction errors, with ADE@1s (0.12m), ADE@2s (0.28m), ADE@3s (0.48m), ADE@4s (0.69m), and ADE@5s (0.86m). Although the latest method SSTT achieves the same ADE@1s compared with the proposed MPCFormer, it has larger prediction error when prediction horizon more than 1 second. Furthermore, MPCFormer maintains a competitive FDE of 2.20 m, highlighting its accuracy. While PECNet achieves the best FDE performance due to its endpoint-conditioned trajectory prediction design, MPCFormer consistently delivers balanced performance across all metrics and time horizons.

#### 6) Qualitative results

This subsection also aims to answer the first question. Figure 9 shows some representative interactive scenarios, demonstrating that the proposed approach has great open-looped prediction performance. Figure 9 (a) and (b) display

the longitudinal-only scenarios which are EAV following in a slower lane and faster lane respectively. These two scenarios highlight the ability of the proposed approach to accurately predict trajectories in both fast and slow lanes at the same time. Figure 9 (c) and (d) are two lane-changing scenarios which are EAV being cut-in and EAV' front SV lane-changing. They demonstrate that the proposed approach shows its superior performance in predicting SV's lateral maneuver.

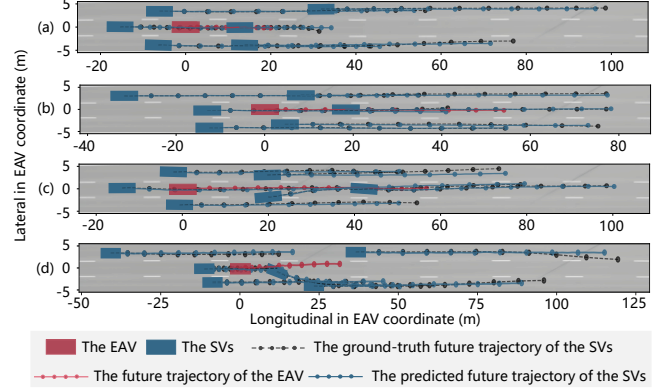


Figure 9 Qualitative results of the proposed approach. (a) EAV following in slower lane; (b) EAV following in faster lane; (c) EAV being cut-in; (d) EAV' front SV lane-changing (The prediction horizon is 5 seconds and the mark points denote the vehicles' position every 0.5 seconds).

#### 7) Socially-aware predictions with explainability

This subsection aims to answer the second question. Figure 10 and TABLE 7 confirms that the proposed MPCFormer actually enable socially-aware predictions with explainability through a random selected case. Figure 10 (a) displays the original prediction which means predicted future trajectories of SVs under the ground-truth future trajectories of the EAV. In Figure 10 (b), this paper modifies the ground-truth future trajectory of the EAV to perform an accelerating and left lane-changing maneuver and analyze how this change affects the predicted future trajectories of the SVs. TABLE 7 shows that the modified trajectory of the EAV demonstrates 5.28 meters and 3.69 meters more than the original trajectory in longitudinal and lateral coordinates. It can be seen that the SVs exhibit relatively steady and lane-consistent predicted motions in Figure 10 (a). In contrast, Figure 10 (b) shows that the Front Vehicle (FV) is significantly influenced by EAV's modified motions, displaying an accelerating trend as an

TABLE 5 Prediction error comparison in different time horizons.

Approach	Prediction error (m)					FDE
	ADE@1s	ADE@2s	ADE@3s	ADE@4s	ADE@5s	
S-GAN	0.19	0.34	0.57	0.83	1.21	2.55
STGAT	0.28	0.58	0.95	1.39	1.88	4.35
STM	0.23	0.54	1.01	1.63	2.08	2.88
HMNet	0.16	0.38	0.62	0.91	1.23	2.95
PECNet	0.28	0.50	0.68	0.82	0.88	<b>0.43</b>
C2F-TP	0.20	0.47	0.78	1.08	1.45	1.36
SSTT	<b>0.12</b>	0.48	0.89	1.34	1.91	2.18
MPCFormer	<b>0.12</b>	<b>0.28</b>	<b>0.48</b>	<b>0.69</b>	<b>0.86</b>	2.20

TABLE 6 Trajectory difference (predicted trajectories after modifying the EAV's future trajectory Figure 10 (b) minus the original predicted trajectories Figure 10 (a)).

Trajectory difference	EAV	FV	RV	LFV	LRV	RFV	RRV
Longitudinal (m)	5.28	4.11	-0.77	1.42	1.62	1.58	0.27
Lateral (m)	3.69	-0.36	-0.25	-0.22	-0.08	-0.12	-0.20
Speed (m/s)	3.11	1.32	-0.10	0.60	0.71	0.63	0.25

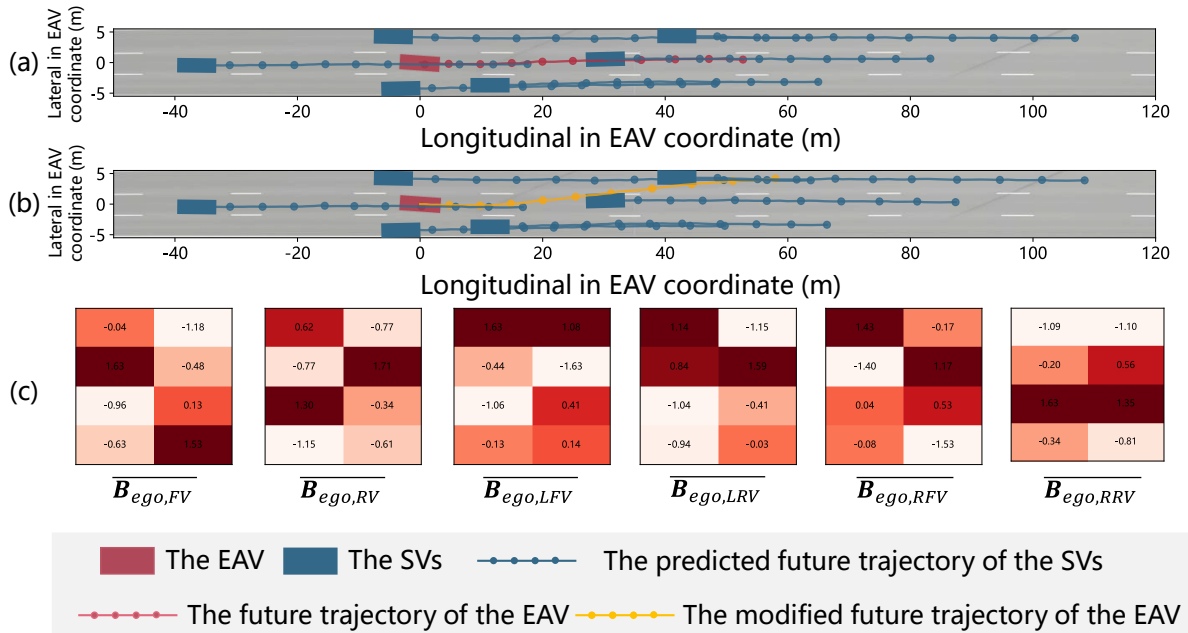


Figure 10 Validation for socially-aware predictions with explainability. (a) original prediction; (b) prediction after modifying EAV's future trajectory; (c) the time-averaged data-driven social interaction matrices defined in 3.2.2. (Additional definition: FV-Front Vehicle, RV-Rear Vehicle, LFV-Left Front Vehicle, LRV-Left Rear Vehicle, RFV-Right Front Vehicle, and RRV-Right Rear Vehicle)

TABLE 7 The Frobenius norm value of data-driven social interaction matrices in Figure 10 (c)

	$B_{ego,FV}$	$B_{ego,RV}$	$B_{ego,LFV}$	$B_{ego,LRV}$	$B_{ego,RFV}$	$B_{ego,RRV}$
<b>Frobenius norm value</b>	0.70	0.26	0.35	0.36	0.36	0.27

TABLE 8 Calibration results of the simulation platform compared to NGSIM

Comparison	NGSIM	The calibrated simulation platform	Error
Main-lane entrance (veh/h)	3240	3247±54	0.21%
On-ramp entrance (veh/h)	503	509±18	1.19%
Main-lane left (veh/h)	3283	3481±70	6.03%
Off-ramp left (veh/h)	271	274±8	1.11%
Traffic average speed (km/h)	34.23	35.18±0.63	2.78%
Traffic lane-changing times	5198	5107±173	1.75%

anticipatory response to the EV's upcoming maneuver. The FV has moved 4.11 meters more than the original predictions and had 1.32 m/s higher speed. In comparison, the Left Front Vehicle (LFV) only exhibits a slight accelerating trend, likely because it is farther ahead and the EAV's lane change occurs behind it. These variations reflect the model's ability to capture socially-aware behaviors. Furthermore, other SVs appear largely unaffected by EV's modified motions. For instance, the Rear Right Vehicle (RRV) shows no notable change, with longitudinal trajectory difference less than 0.3 meter. This aligns with the common sense that a vehicle's acceleration and lane-change maneuver have minimal impact on vehicles right behind it.

Figure 10 (c) and TABLE 7 validates the explainability of the prediction with the data-driven social interaction matrices defined in Section 3.2.2. For instance,  $B_{ego,FV}$  explicitly represents the time-averaged social interaction effect from the EAV to the FV. These matrices vary across vehicle pairs, indicating that the model captures distinct and directional social interaction patterns between different vehicles. Moreover, TABLE 7 shows that the social

interaction strength between the EAV and the FV exhibits the highest norm value (0.70), indicating that the EAV exerts the most significant influence on the FV. In contrast, social interactions with rear-side vehicles (e.g., RV and RRV) show much lower norm values (0.26 and 0.27), suggesting relatively weaker social interaction influence. The explicit social interaction dynamics modeling paradigm design enhances explainability by providing explicit representations of how each vehicle influences others over time.

### B. Close-looped planning performance validation

The close-looped planning performance validation aims to answer the following questions: i) How is the proposed MPCFormer's planning capability compared to existing approaches? ii) Can the proposed MPCFormer enable explainable socially-aware planning? iii) Can the proposed MPCFormer enhance driving efficiency but not be unsafe?

#### 1) Simulation platform for close-looped driving

The planning simulation platform is Vissim [41] which is a highly realistic traffic and vehicle dynamics simulation software. The reason why this paper builds a new simulation

environment instead of replaying NGSIM dataset directly like many current researches [6][23] is that:

- If replaying NGSIM data directly, SVs cannot respond to the EAV’s planned motion, which called “non-reactive” vehicles. By contrast, Vissim has highly developed reaction models for SVs. Hence, it can portray realistic social interactions between EAV and SVs.

- Vissim can support flexible sensitivity analysis but replaying NGSIM data cannot.

By calibrating traffic parameters, this paper sets up a simulation environment similar to NGSIM dataset. The calibration results are shown in TABLE 8.

### 2) Test scenario

As illustrated in Figure 11, the test scenario takes place on a section of interweaving traffic on US Highway 101. The goal of EAV is to navigate and successfully complete an off-ramp maneuver. The start position and the target lane of EAV are marked in Figure 11. The EAV must complete three consecutive lane changes within a short distance, leading to intense interactions, making this a challenging scenario. Six test cases are designed as shown in TABLE 9. Sensitivity analysis is conducted in terms of traffic congestion levels (v/c ratio of 0.4, 0.6, and 0.8) and driving styles (aggressive and normal).

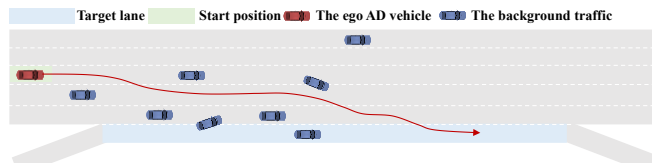


Figure 11 The test scenario: EAV off-ramp in US Highway 101.

TABLE 9 Case definitions

	v/c = 0.4	v/c = 0.6 (NGSIM)	v/c = 0.8
Aggressive (NGSIM)	Case1	<b>Case2</b>	Case3
Normal	Case4	Case5	Case6

### 3) Planners for comparison

Three types of socially-aware planners are considered:

- **The PAS planner:** A traditional **P**assively **S**ocially-**A**ware (PAS) approach designed based on the Intelligent

Driver Model (IDM) [42] and Minimizing Overall Braking Induced by Lane-change (MOBIL) model [43].

- **The NS planner:** A Proximal Policy Optimization (PPO) reinforcement learning approach for lane-changing [44]. This approach is a classic **N**eutrally **S**ocially-**A**ware (NS) approach and has gained high academic impact since its publication. The reward function and parameter settings remain the same with the original paper.

- **The proposed planner:** This planner is the proposed approach MPCFormer. It can be seen as a **P**roactively **S**ocially-**A**ware (PRS) approach.

### 4) Measures of effectiveness

Measures of effectiveness (MOE) are adopted as follows.

**Success / Failure / Collision rate.** Success rate means the percentage of successful off-ramps among 100 random tests in different cases; failure rate means the percentage of missed off-ramps but not colliding; collision rate means the percentage of collisions during the off-ramp; **Vehicle trajectories.** The sampled vehicle trajectories of EAV and SVs used for validating planning socially-aware capability and explainability; **Frobenius norm** of the data-driven social interaction matrices. The higher value of the Frobenius norm explains the higher social interaction strength between vehicles; **Off-ramp duration.** Average length of time required for EAV off-ramp over random tests; **Average speed.** EAV’s average speed over random tests; **Actual safety.** The average value of EAV’s time headway under a predefined safety threshold is used to measure actual risk; **Perceived safety.** The perceived risk is quantified through frequency-domain analysis [45] of the EAV’s time headway. The magnitude of power across frequencies reflects the oscillation intensity and stability of the EAV’s behavior; **Speed distribution.** Speed distribution of EAV in different cases; **Lane-change distance.** The longitudinal distance required for one lane-change of EAV in different cases.

### 5) Overall planning capability validation

The results confirm that the proposed planner outperforms the PAS and NS planners, further indicating the advantage of

TABLE 10 The success/failure/collision rate comparison in different cases.

		Success (%)	Failure (%)	Collision (%)
Case 1	PAS planner	39	44	17
	NS planner	72	9	19
	The proposed planner	<b>96</b>	4	0
Case 2	PAS planner	31	46	23
	NS planner	69	9	22
	The proposed planner	<b>94</b>	6	0
Case 3	PAS planner	29	49	22
	NS planner	56	12	32
	The proposed planner	<b>90</b>	8	2
Case 4	PAS planner	49	38	13
	NS planner	82	6	12
	The proposed planner	<b>99</b>	1	0
Case 5	PAS planner	49	35	16
	NS planner	76	8	16
	The proposed planner	<b>95</b>	5	0
Case 6	PAS planner	39	46	15
	NS planner	71	10	19
	The proposed planner	<b>94</b>	5	1

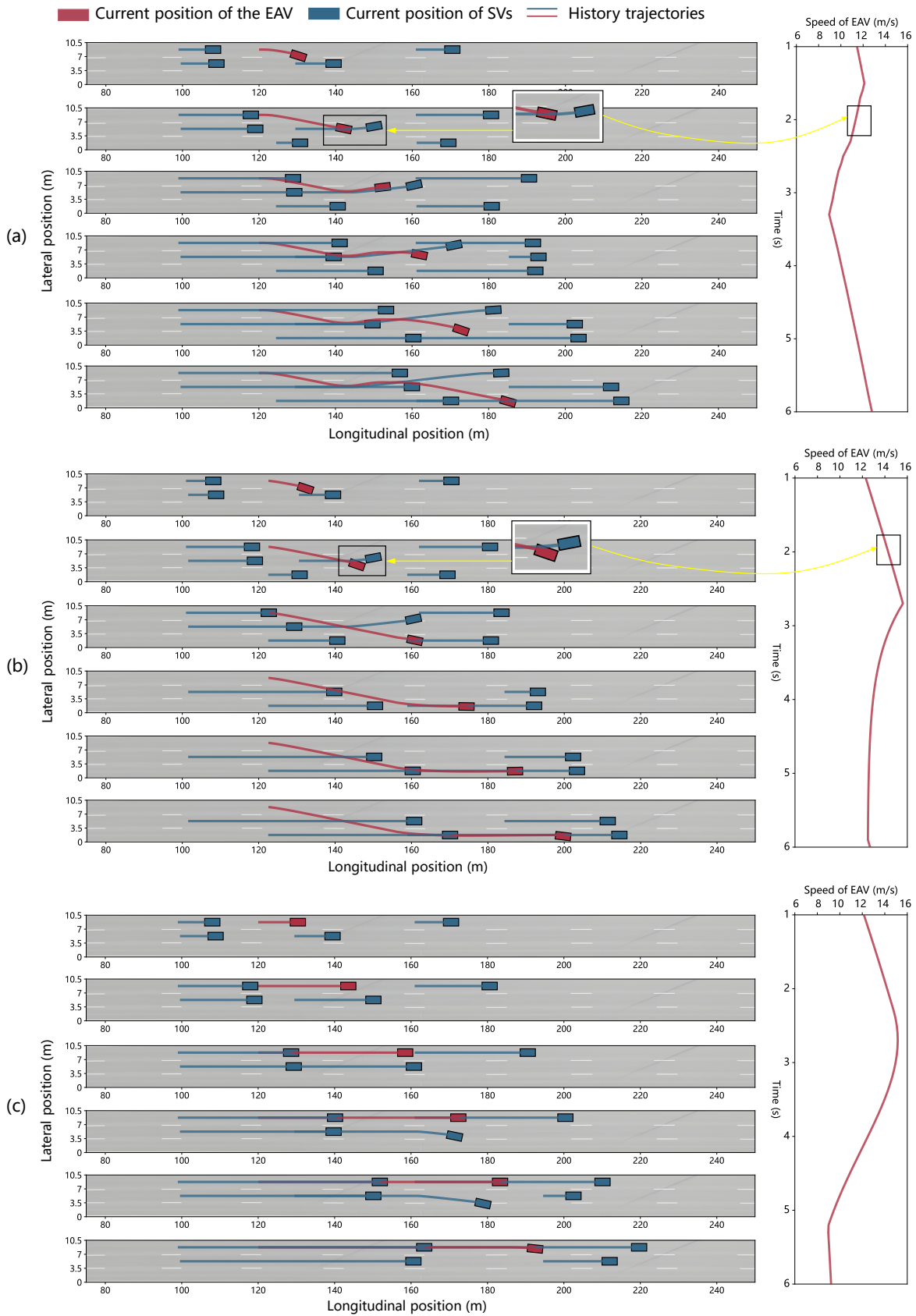


Figure 12 The planning capability comparison in a randomly selected case. (a) the proposed planner; (b) the NS planner; (c) the PAS planner. (The trajectories from top to bottom corresponds to timestep at 1s to 6s.)

TABLE 11 The time varied Frobenius norm value of the data-driven social interaction matrices.

Social interaction with:	Frobenius norm value					
	FV	RV	LFV	LRV	RFV	RRV
Time@1s	1.05	0.41	0.33	-	-	0.40
Time@2s	1.21	0.36	0.32	0.29	0.36	0.71
Time@3s	1.29	0.36	0.33	0.28	0.35	0.65
Time@4s	0.65	0.37	0.99	0.29	0.36	0.76
Time@5s	0.43	0.36	0.32	0.28	0.35	0.85
Time@6s	0.37	0.48	0.35	0.28	-	-

evidenced by the off-ramp success rate in TABLE 10. The proposed planner achieves a superior success rate of over 90% across all cases. In comparison, the NS planner outperforms the PAS planner, with an average success rate of 71% versus 39.3%. It demonstrates the proposed planner has advantages in highly interactive scenarios. Meanwhile, the proposed approach achieves the lowest collision rate with an average of 0.5%. This is attributed to the proposed planner’s ability of considering SVs’ reactions while hard safety constraints. Furthermore, it can be found that all three planners have the highest success rate in case 3 and the lowest success rate in case 4 because case 3 is the most challenging scenario, case 4 the opposite.

6) *Explainable socially-aware capability validation*

Furthermore, this paper randomly selects a case to analyze the explainable socially-aware planning capability as shown in Figure 13. In this case, the initial traffic conditions and initial positions of the EAV are identical for all three planners. In Figure 13 (a), the EAV decelerates and return to the original lane at around 2 s when attempting a lane change. Qualitatively, it can be seen that EAV’s Front Vehicle (FV) is also attempting a lane change. EAV is aware of the risk and chooses to avoid it. When the FV drives away, the EAV retries to accelerate and cut in for reaching the target lane. This case demonstrates the socially-aware planning capability of the EAV. Furthermore, the social interaction process of Figure 13 (a) is also explainable. TABLE 11 shows the time varied Frobenius norm value of the data-driven social interaction matrices when EAV interacting with other SVs. It can be seen that when considering social interaction with FV, the value is high and increases in first 3 seconds, which is align with the interaction process with FV in Figure 13 (a). The value is also high when interacting with RRV at 5th seconds. It makes sense as the EAV s cutting in front of the RRV. TABLE 11 demonstrates that the Frobenius norm value of the data-driven social interaction matrices can explain the social interaction process of the proposed planner.

In Figure 13 (b), the EAV equipped with the NS planner changes lanes with on hesitation. Compared with the proposed planner, at the 2nd seconds, the NS planner didn’t choose to decelerate and nearly result in a collision with the FV. This case indicates that the NS planner lacks enough socially-aware planning capability in a complex traffic environment. In Figure 13 (c), the PAS planner was unable to execute a lane change throughout the scenario due to its passive and conservative reaction nature.

7) *Driving efficiency validation*

The results confirm that the proposed planner improves driving efficiency. As illustrated in Figure 13, the proposed planner educes off-ramp duration compared to other planners. Compared to the NS planner, the proposed planner can save

off-ramp duration by up to 11.23s and an average of 9.15s. With respect to the PAS planner, the proposed planner saves off-ramp duration by up to 14.62s and an average of 9.19s. These improvements are due to the planner’s proactive motions that account for interactions, boosting efficiency. Additionally, the NS planner spends less duration than the PAS planner in case 1 to case 3, opposite in case 4 to case 6. This indicates that the NS planner is more capable of handling traffic with aggressive driving styles compared with the PAS planner.

Figure 14 shows the EAV average speed comparison in different cases. Compared with the NS planner, the proposed planner achieves a 15.75% improvement in average speed. Similarly, it outperforms the PAS planner by 15.23% in average speed. However, the average speed of the proposed planner decreases when faced with larger v/c ratios and more aggressive driving styles. It is obvious that dense and aggressive traffic causes dense interactions, leading to a lower average speed. An interesting observation is that although the NS planner exhibits lower average speed than the PAS planner in Case 1 to Case 3, it demonstrates shorter off-ramp durations. This indicates that the NS planner is more competitive in certain aspects, as it is able to perform lane changes more quickly and efficiently than the PAS planner.

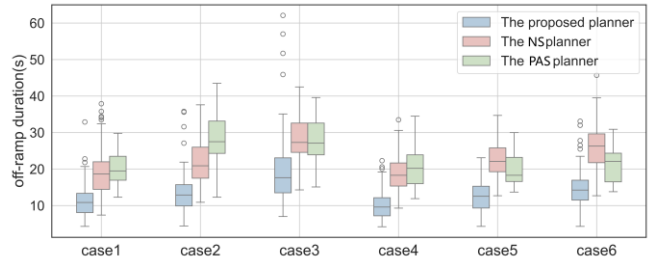


Figure 13 The off-ramp duration of EAV in different cases.

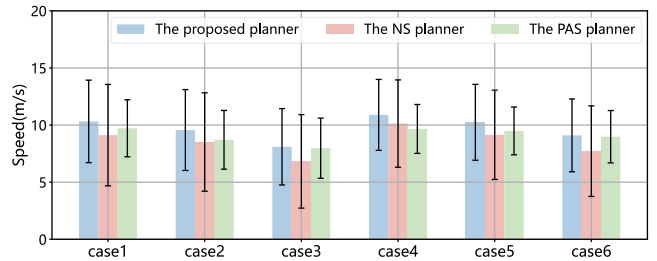


Figure 14 The average speed of EAV in different cases.

8) *Driving safety validation results*

The results confirm that the proposed planner effectively ensures safety. The collision rates shown in TABLE 10 indicates the proposed planner has the lowest risk to collide. Meanwhile, in those “no-collision” tests, the proposed planner achieves superior actual safety performance by the largest average time headway in Case1(0.39, 0.30, 0.34),

Case4 (**0.43**, 0.20, 0.43), and Case6 (**0.43**, 0.15, 0.31) as shown in Figure 15. This is because the proposed planner proactively interacts with surrounding vehicles to reduce risky behaviors. However, the PAS planner outperforms in Case2 (0.25, 0.22, **0.31**), Case3 (0.34, 0.20, **0.42**), and Case5 (0.34, 0.27, **0.44**). This can be attributed to its “passively reaction” nature, prioritizing safety with greater confidence which has benefit in highly interactive scenarios like case 2 and case 3. Meanwhile, the NS planner displays the worst safety performance across all cases. This reflects the limitation that the pure learning-based approaches are often hard to guarantee safety.

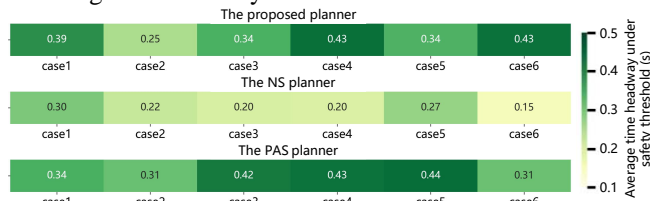


Figure 15 The EAV average time headway comparison.

The perceived safety is evaluated based on the frequency-domain analysis of the EAV’s time headway, as illustrated in Figure 17. The frequency-domain analysis is based on the discrete Fourier transform (DFT), which is efficiently computed using the Fast Fourier Transform (FFT) algorithm [45]. It shows that the proposed planner enhances perceived safety by reducing the frequency of time headway oscillation. Compared to the NS planner and the PAS planner, the proposed planner consistently demonstrates lower power magnitudes at higher frequencies (more than 1 Hz), indicating smoother and more stable time headway with fewer rapid oscillations. In contrast, the PAS planner shows significantly higher spectral power in mid-to-high frequency bands, especially in Case 3 and Case 5. This implies that the PAS planner tends to produce frequent and abrupt adjustments in response to traffic, likely due to the lack of proactive or anticipatory interaction modeling. The NS planner exhibits intermediate performance, with lower oscillation levels than the PAS planner, but still less stable than the proposed planner. This suggests that while learning-based strategies offer moderate adaptability, they may lack the consistent smoothness achieved by incorporating physical and socially-aware mechanisms.

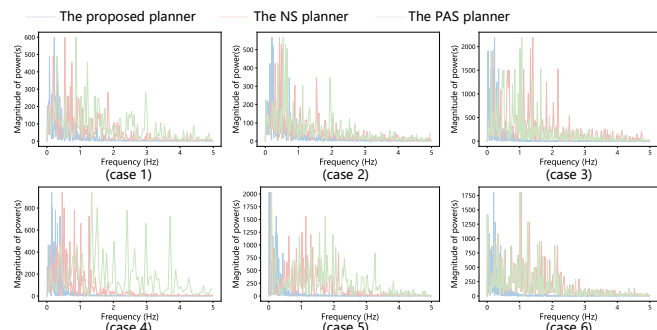


Figure 16 Frequency analysis of EAV’s time headway comparison in different cases.

### 9) Driving flexibility validation results

The results confirm that the proposed planner demonstrates high flexibility in the highly interactive traffic scenarios. Figure 17 compares the speed distribution across different cases. It can be seen that the speed distributions of

the proposed planner across different cases are wider and more uniform, with no significant peaks or valleys. This flexibility reflects the proposed planner can adjust speed as needed when interacting with other vehicles, either by seizing lane-change opportunities or yielding for safety. In contrast, the PAS planner displays noticeable distribution peaks across different cases, suggesting a tendency to maintain a fixed speed due to its limited ability to engage in proactive, interaction-aware driving. The NS planner also demonstrates a relatively uniform speed distribution, highlighting that pure learning-based approaches possess inherent advantages in driving flexibility. In addition, all planners exhibit more concentrated speed distributions in Case 4. This is expected, as lower interaction intensity in this scenario reduces speed oscillations and leads to more stable driving behavior.

Figure 18 compares the lane change distance distribution across different cases. The commonality among the six cases is that the PAS planner has obviously larger lane change distance. The proposed planner saves 49.01% of lane change distance on average compared with the PAS planner. As the PAS planner relies on predefined rules and passively reacts to surrounding vehicles, resulting in struggling in interactive scenarios. Compared with the NS planner, the proposed planner has wider box of the lane change distribution in Case 1 to Case 3, but the opposite in Case 4 to Case 6. This indicates the proposed planner is more competitive and can adjust its lane change distance flexibly to obtain better planning capability in the aggressive traffic.

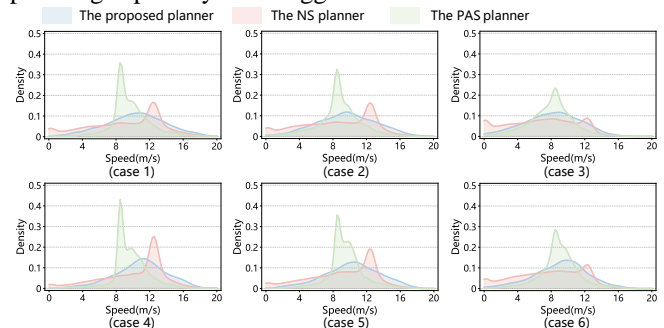


Figure 17 The speed distribution comparison in different cases.

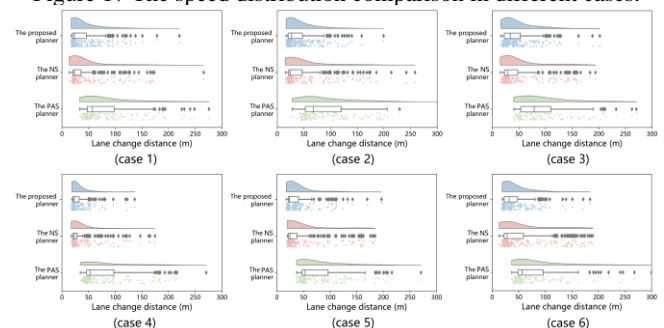


Figure 18 The lane change distance comparison in different cases.

## IV. CONCLUSION

This paper introduces *MPCFormer*, an explainable socially-aware autonomous driving approach with physics-informed and data-driven coupled social interaction dynamics. In this model, the dynamics are formulated into a discrete space-state representation, which embeds physics priors to enhance modeling explainability. The dynamics coefficients are learned from naturalistic driving data via a Transformer-

based encoder-decoder architecture. To the best of our knowledge, MPCFormer is the first approach to explicitly model the dynamics of multi-vehicle social interactions. By integrating the learned social interaction dynamics into MPC planning based on a leader-follower game framework, the AD vehicle can generate manifold, human-like behaviors when interacting with surrounding traffic while mitigate the potential safety risks typically associated with purely learning-based approaches. Open-looped prediction and close-looped planning results demonstrate that:

- In open-loop prediction, the proposed MPCFormer achieves the lowest SV trajectory prediction error among state-of-the-art approaches, achieving an ADE as low as 0.86 m over a long prediction horizon of 5 seconds.

- In close-looped planning, the proposed MPCFormer ensures highest overall planning capability with an average success rate of 94.67%. The proposed MPCFormer reduces the collision rate from 21.25% to 0.5%. It also has validated explainable socially-aware planning capability.

- The proposed MPCFormer also demonstrates efficiency gains of up to 15.75% and 15.23% compared to the two baseline planners and ensures perceived and actual safety. Furthermore, the proposed MPCFormer is more flexible in interactive driving scenarios with more uniform speed distribution and smaller lane-change distance.

#### REFERENCES

- [1] Z. Zhang, H. Liu, M. Lei, X. Yan, M. Wang, and J. Hu, "Review on the impacts of cooperative automated driving on transportation and environment," *Transportation Research Part D: Transport and Environment*, vol. 115, p. 103607, 2023.
- [2] S. Teng et al., "Motion planning for autonomous driving: The state of the art and future perspectives," *IEEE Transactions on Intelligent Vehicles*, vol. 8, no. 6, pp. 3692-3711, 2023.
- [3] J. Wu, C. Huang, H. Huang, C. Lv, Y. Wang, and F.-Y. Wang, "Recent advances in reinforcement learning-based autonomous driving behavior planning: A survey," *Transportation Research Part C: Emerging Technologies*, vol. 164, p. 104654, 2024.
- [4] S. Feng et al., "Dense reinforcement learning for safety validation of autonomous vehicles," *Nature*, vol. 615, no. 7953, pp. 620-627, 2023.
- [5] W. Wang, L. Wang, C. Zhang, C. Liu, and L. Sun, "Social interactions for autonomous driving: A review and perspectives," *Foundations and Trends® in Robotics*, vol. 10, no. 3-4, pp. 198-376, 2022.
- [6] Z. Huang, H. Liu, J. Wu, and C. Lv, "Differentiable Integrated Motion Prediction and Planning With Learnable Cost Function for Autonomous Driving," *IEEE Transactions on Neural Networks and Learning Systems*, pp. 1-15, 2023, doi: 10.1109/TNNLS.2023.3283542.
- [7] J. Eggert, "Predictive risk estimation for intelligent ADAS functions," in *17th International IEEE Conference on Intelligent Transportation Systems (ITSC)*, 8-11 Oct. 2014 2014, pp. 711-718, doi: 10.1109/ITSC.2014.6957773.
- [8] B. Li, Z. Yin, Y. Ouyang, Y. Zhang, X. Zhong, and S. Tang, "Online trajectory replanning for sudden environmental changes during automated parking: A parallel stitching method," *IEEE Transactions on Intelligent Vehicles*, vol. 7, no. 3, pp. 748-757, 2022.
- [9] P. Li, X. Pei, Z. Chen, X. Zhou, and J. Xu, "Human-like motion planning of autonomous vehicle based on probabilistic trajectory prediction," *Applied Soft Computing*, vol. 118, p. 108499, 2022.
- [10] M. Werling, J. Ziegler, S. Kammel, and S. Thrun, "Optimal trajectory generation for dynamic street scenarios in a Frenet Frame," in *2010 IEEE International Conference on Robotics and Automation*, 3-7 May 2010 2010, pp. 987-993, doi: 10.1109/ROBOT.2010.5509799.
- [11] S. Sheng, P. Yu, D. Parker, M. Kwiatkowska, and L. Feng, "Safe POMDP Online Planning Among Dynamic Agents via Adaptive Conformal Prediction," *IEEE Robotics and Automation Letters*, vol. 9, no. 11, pp. 9946-9953, 2024, doi: 10.1109/LRA.2024.3468092.
- [12] C. Hubmann, J. Schulz, G. Xu, D. Althoff, and C. Stiller, "A Belief State Planner for Interactive Merge Maneuvers in Congested Traffic," in *2018 21st International Conference on Intelligent Transportation Systems (ITSC)*, 4-7 Nov. 2018 2018, pp. 1617-1624, doi: 10.1109/ITSC.2018.8569729.
- [13] J. Zhou, B. Olofsson, and E. Frisk, "Interaction-aware motion planning for autonomous vehicles with multi-modal obstacle uncertainty predictions," *IEEE Transactions on Intelligent Vehicles*, 2023.
- [14] C. Wei, Y. He, H. Tian, and Y. Lv, "Game Theoretic Merging Behavior Control for Autonomous Vehicle at Highway On-Ramp," *IEEE Transactions on Intelligent Transportation Systems*, vol. 23, no. 11, pp. 21127-21136, 2022, doi: 10.1109/TITS.2022.3174659.
- [15] L. Crosato, K. Tian, H. P. H. Shum, E. S. L. Ho, Y. Wang, and C. Wei, "Social Interaction-Aware Dynamical Models and Decision-Making for Autonomous Vehicles," *Advanced Intelligent Systems*, vol. 6, no. 3, 2023, doi: 10.1002/aisy.202300575.
- [16] L. Le Mero, D. Yi, M. Dianati, and A. Mouzakitis, "A survey on imitation learning techniques for end-to-end autonomous vehicles," *IEEE Transactions on Intelligent Transportation Systems*, vol. 23, no. 9, pp. 14128-14147, 2022.
- [17] K. Chitta, A. Prakash, B. Jaeger, Z. Yu, K. Renz, and A. Geiger, "TransFuser: Imitation With Transformer-Based Sensor Fusion for Autonomous Driving," *IEEE Transactions on Pattern Analysis and Machine Intelligence*, vol. 45, no. 11, pp. 12878-12895, 2023, doi: 10.1109/TPAMI.2022.3200245.
- [18] E. Bronstein et al., "Hierarchical model-based imitation learning for planning in autonomous driving," in *2022 IEEE/RSJ International Conference on Intelligent Robots and Systems (IROS)*, 2022: IEEE, pp. 8652-8659.
- [19] F. Ye, X. Cheng, P. Wang, C. Y. Chan, and J. Zhang, "Automated Lane Change Strategy using Proximal Policy Optimization-based Deep Reinforcement Learning," in *2020 IEEE Intelligent Vehicles Symposium (IV)*, 19 Oct.-13 Nov. 2020 2020, pp. 1746-1752, doi: 10.1109/IV47402.2020.9304668.
- [20] J. Hu, X. Yan, T. Xu, and H. Wang, "Automated Driving with Evolution Capability: A Reinforcement Learning Method with Monotonic Performance Enhancement," *arXiv preprint arXiv:2412.10822*, 2024.
- [21] M. Zhu, Y. Wang, Z. Pu, J. Hu, X. Wang, and R. Ke, "Safe, efficient, and comfortable velocity control based on reinforcement learning for autonomous driving," *Transportation Research Part C: Emerging Technologies*, vol. 117, p. 102662, 2020/08/01/ 2020, doi: <https://doi.org/10.1016/j.trc.2020.102662>.
- [22] S. Ross, G. Gordon, and D. Bagnell, "A reduction of imitation learning and structured prediction to no-regret online learning," in *Proceedings of the fourteenth international conference on artificial intelligence and statistics, 2011: JMLR Workshop and Conference Proceedings*, pp. 627-635.
- [23] R. Hu et al., "Imitation learning decision with driving style tuning for personalized autonomous driving," in *International Conference on Database Systems for Advanced Applications*, 2024: Springer, pp. 220-231.
- [24] Z. Zhang, X. Yan, H. Wang, C. Ding, L. Xiong, and J. Hu, "No more road bullying: An integrated behavioral and motion planner with proactive right-of-way acquisition capability," *Transportation Research Part C: Emerging Technologies*, vol. 156, p. 104363, 2023/11/01/ 2023, doi: <https://doi.org/10.1016/j.trc.2023.104363>.
- [25] L. Gharavi, A. Dabiri, J. Verkuiljen, B. De Schutter, and S. Baldi, "Proactive emergency collision avoidance for automated driving in highway scenarios," *IEEE Transactions on Control Systems Technology*, 2024.
- [26] J. Hu et al., "Anti-bullying Adaptive Cruise Control: A proactive right-of-way protection approach," *arXiv preprint arXiv:2412.12197*, 2024.
- [27] J. Fan, Y. Ni, D. Zhao, P. Hang, and J. Sun, "Toward Proactive-Aware Autonomous Driving: A Reinforcement Learning Approach Utilizing Expert Priors During Unprotected Turns," *IEEE Transactions on Intelligent Transportation Systems*, 2024.
- [28] J. Goldenbott and K. Leung, "Legible and proactive robot planning for prosocial human-robot interactions," *arXiv preprint arXiv:2404.03734*, 2024.
- [29] R. Rajamani, "Lateral Vehicle Dynamics," in *Vehicle Dynamics and Control*, R. Rajamani Ed. Boston, MA: Springer US, 2012, pp. 15-46.
- [30] A. Vaswani, "Attention is all you need," *Advances in Neural Information Processing Systems*, 2017.

- [31] F. Etro, "Stackelberg Competition with Endogenous Entry," *The Economic Journal*, vol. 118, no. 532, pp. 1670-1697, 2008, doi: 10.1111/j.1468-0297.2008.02185.x.
- [32] M. Coccioni and L. Fiaschi, "The Big-M method with the numerical infinite M," *Optimization Letters*, vol. 15, no. 7, pp. 2455-2468, 2021.
- [33] B. Coifman and L. Li, "A critical evaluation of the Next Generation Simulation (NGSIM) vehicle trajectory dataset," *Transportation Research Part B: Methodological*, vol. 105, pp. 362-377, 2017/11/01/2017, doi: <https://doi.org/10.1016/j.trb.2017.09.018>.
- [34] A. Gupta, J. Johnson, L. Fei-Fei, S. Savarese, and A. Alahi, "Social gan: Socially acceptable trajectories with generative adversarial networks," in *Proceedings of the IEEE conference on computer vision and pattern recognition*, 2018, pp. 2255-2264.
- [35] A. Mohamed, K. Qian, M. Elhoseiny, and C. Claudel, "Social-stgcnn: A social spatio-temporal graph convolutional neural network for human trajectory prediction," in *Proceedings of the IEEE/CVF conference on computer vision and pattern recognition*, 2020, pp. 14424-14432.
- [36] T. Yu, F. Hui, X. Shuoshuo, W. Mengyuan, and X. Lingyang, "Vehicle Trajectory Prediction Based on Spatial-aware Transformer," in *2023 IEEE 11th International Conference on Information, Communication and Networks (ICICN)*, 2023: IEEE, pp. 884-889.
- [37] Q. Xue, S. Li, X. Li, J. Zhao, and W. Zhang, "Hierarchical motion encoder-decoder network for trajectory forecasting," *arXiv preprint arXiv:2111.13324*, 2021.
- [38] K. Mangalam *et al.*, "It is not the journey but the destination: Endpoint conditioned trajectory prediction," in *Computer Vision—ECCV 2020: 16th European Conference, Glasgow, UK, August 23–28, 2020, Proceedings, Part II 16*, 2020: Springer, pp. 759-776.
- [39] Z. Wang, H. Miao, S. Wang, R. Wang, J. Wang, and J. Zhang, "C2f-tp: A coarse-to-fine denoising framework for uncertainty-aware trajectory prediction," in *Proceedings of the AAAI Conference on Artificial Intelligence*, 2025, vol. 39, no. 12, pp. 12810-12817.
- [40] X. Li, J. Zhang, J. Chen, and P. Qian, "Interaction-Aware Trajectory Prediction Method Based on Sparse Spatial-Temporal Transformer for Internet of Vehicles," *IEEE Transactions on Intelligent Transportation Systems*, 2025.
- [41] J. Hu *et al.*, "A Simulation Platform for Truck Platooning Evaluation in an Interactive Traffic Environment," *IEEE Transactions on Intelligent Transportation Systems*, 2024.
- [42] M. Liebner, M. Baumann, F. Klanner, and C. Stiller, "Driver intent inference at urban intersections using the intelligent driver model," in *2012 IEEE Intelligent Vehicles Symposium*, 3-7 June 2012 2012, pp. 1162-1167, doi: 10.1109/IVS.2012.6232131.
- [43] A. Kesting, M. Treiber, and D. Helbing, "General Lane-Changing Model MOBIL for Car-Following Models," *Transportation Research Record*, vol. 1999, no. 1, pp. 86-94, 2007/01/01 2007, doi: 10.3141/1999-10.
- [44] F. Ye, X. Cheng, P. Wang, C. Y. Chan, and J. Zhang, "Automated Lane Change Strategy using Proximal Policy Optimization-based Deep Reinforcement Learning," in *2020 IEEE Intelligent Vehicles Symposium (IV)*, 19 Oct.-13 Nov. 2020 2020, pp. 1746-1752, doi: 10.1109/IV47402.2020.9304668.
- [45] M. Frigo and S. G. Johnson, "FFTW: An adaptive software architecture for the FFT," in *Proceedings of the 1998 IEEE International Conference on Acoustics, Speech and Signal Processing, ICASSP98 (Cat. No. 98CH36181)*, 1998, vol. 3: IEEE, pp. 1381-1384.



**Jia Hu** (Senior Member, IEEE) is currently working as a Zhongte Distinguished Chair of Cooperative Automation with the College of Transportation Engineering, Tongji University. Before joining Tongji University, he was a Research Associate with the Federal Highway Administration (FHWA), USA. He is an Editorial Board Member of the *Journal of Intelligent Transportation Systems* and the *International Journal of Transportation Science and Technology*. He is a member of TRB (a Division of the National Academies) Vehicle Highway Automation Committee, the Freeway Operations Committee, Simulation subcommittee of Traffic Signal Systems Committee, and the Advanced Technologies Committee of the ASCE Transportation and Development Institute. He is the Chair of the Vehicle Automation and Connectivity Committee of the World Transport

Convention. He is an Associate Editor of the *American Society of Civil Engineers Journal of Transportation Engineering* and *IEEE OPEN JOURNAL OF INTELLIGENT TRANSPORTATION SYSTEMS*.



**Zhaxi Lian** was born in Shanxi, China. He received the bachelor's degree in transportation engineering from College of Transportation, Tongji University, Shanghai, China, in 2023. He is currently pursuing the Ph.D. degree with Key Laboratory of Road and Traffic Engineering of the Ministry of Education, Tongji University. His main research interests include data-driven control, end-to-end autonomous driving and vision language action models.



**Xuerun Yan** received his B.S. degree in traffic engineering from Southeast University in 2021. He currently works as a research assistant with the Key Laboratory of Road and Traffic Engineering, Ministry of Education, Tongji University, Shanghai, China. His research interests are in the areas of AV simulation, AV planning, and cooperative driving.



**Ruiang Bi** received the bachelor's degree in transportation engineering from Tongji University, Shanghai China, in 2024. He is currently working toward the master's degree with Tongji University, Shanghai, China. His main research interests include cooperative automation, optimal control, decision making, and behavioral planning.



**Dou Shen** received a Ph.D. from the Hong Kong University of Science and Technology, and currently serves as executive vice president of Baidu and the president of Baidu AI Cloud Group. Dr. Shen joined Baidu in 2012 and has served in various management roles, including web search, display advertising, the financial services group and mobile products. Dr. Shen has published more than 40 papers in international conferences and journals, and held multiple patents on Internet search and computational advertising. Currently, he serves as the Vice President of SIGKDD China Chapter, the Dean of the School of Artificial Intelligence at North China Electric Power University, the independent director of COSCO Shipping Holdings Co., Ltd., and the director of companies such as China Unicom, CITIC AIBANK, Neusoft, and iQiyi.



**Yu Ruan** graduated from Ningxia University and holds an EMBA from China Europe International Business School (CEIBS). She is currently Vice President of Baidu and General Manager of Baidu Intelligent Cloud Application Product Division. With over a decade of experience in Internet product operations, Yuan Yu is an industry expert in product management, operations, and brand marketing. She has extensive management experience and has led her teams to achieve multiple business breakthroughs and innovative transformations.



**Haoran Wang** received the bachelor's degree in transportation engineering from Tongji University, Shanghai, China, in 2017, and the Ph.D. degree from Tongji University in 2022. He is currently a Postdoctoral Researcher with the College of Transportation Engineering, Tongji University. He is a researcher on vehicle engineering, majoring in intelligent vehicle control and cooperative automation. Dr. Wang served the *IEEE TRANSACTIONS ON INTELLIGENT VEHICLES*, *IEEE TRANSACTIONS ON INTELLIGENT TRANSPORTATION SYSTEMS*, *Journal of Intelligent Transportation Systems*, and *IET Intelligent Transport Systems* as peer reviewers with a good reputation.